Lanthanides in Non-Oxide Glasses

Jean-Luc Adam

Laboratoire des Verres and Céramiques, Institut de Chimie de Rennes, Université de Rennes 1, UMR-CNRS 6512, Campus Scientifique de Beaulieu, 35042 Rennes Cedex, France

Received February 14, 2002

Contents

I. Introduction

Lanthanide components are constituents of major importance in the chemistry of non-oxide glasses. Even though they cannot form glasses by themselves, lanthanides may enter the vitreous network in association with glass-forming components such as ZrF_4 in fluoride glasses or Ga_2S_3 in sulfides. In those cases, lanthanides are necessary to the formation of thermally stable matrices, that is, glasses with large temperature differences between the glass transition and crystallization. In a second category, lanthanides are not present in the initial glass composition. However, they can still be incorporated as dopants in the vitreous network and act as active centers for luminescence.

Non-oxide glasses can be divided in halide glasses and chalcogenide glasses. Halide glasses are essentially fluorides based on zirconium or indium as glass formers associated with barium fluoride, Ba^{2+} ions acting as glass modifiers. Optical fibers and planar waveguides containing paramagnetic lanthanide ions can be elaborated with fluoride glasses. Thus, efficient fluoride fiber lasers and fiber amplifiers have been demonstrated at wavelengths not available with oxide glasses. Chalcogenide glasses containing lanthanides are sulfides and selenides. In the same way as for fluorides, the search for such glasses is motivated by optical applications that can be either passive—with the transmission of infrared signals through lenses or fibers—or active—with the photoluminescence of paramagnetic lanthanides. Due to low phonon energies, chalcogenides permit luminescence of lanthanide ions with high quantum efficiency. Thus, electronic transitions, especially in the infrared, which do not occur in fluoride or oxide glasses, can be observed in chalcogenides.

This paper deals with the chemical preparation, properties, and applications of non-oxide glasses containing lanthanide ions.

Jean-Luc Adam received the Ph.D. degree in chemistry from the University of Rennes, France, in 1983. After a 1-year postdoctoral appointment at Oklahoma State University, Stillwater, OK, he joined the Centre National de la Recherche Scientifique in France in 1985. Since then, his research has been devoted essentially to the chemistry of non-oxide glasses and to the spectroscopy of optically active ions for applications in telecommunications and solid-state laser systems. Appointed Directeur de Recherche in 1999, he is currently head of the Optical Glasses group in the Glass & Ceramics Laboratory at the University of Rennes.

II. Lanthanide-Containing Halide Glasses

1. Chemical Composition and Glass Synthesis

Halide glasses containing lanthanides are essentially fluoride glasses, the compositions of which are

10.1021/cr010305b CCC: $39.75
Published on Web 05/14/2002

given in Table 1. Based on zirconium fluoride, ZBLAN fluorozirconate glasses contain also 4 mol % lanthanum fluoride, which is essential to glass formation. A vitreous phase is found in the ZrF_4-BaF_2 binary system if fast quenching is used for cooling the mixture. In that system, ZrF_4 (60−70%) acts as the glass former; large Ba^{2+} ions (40−30%) are the network modifiers, introducing disorder in the matrix. Lanthanum, as well as aluminum, is a strong stabilizer of the vitreous state in fluorozirconate glasses, allowing glass formation by gentle cooling. Further addition of a second glass-network modifier (Na^+) reduces the tendency of fluorozirconates to crystallize, which makes ZBLAN the most stable fluoride glass, suitable for fiber drawing.

Fluoroindate glasses are based on barium, indium, and gallium fluorides, in association with zinc fluoride. BIG glass, shown in Table 1, is representative of this family, where the glass formers are InF_3 and GaF_3.[1] One should note the relatively high concentration of rare-earth fluorides, typically in the 15% range. In addition to being essential to glass formation, such high concentrations allow more flexibility in rare-earth combinations for spectroscopic studies, especially for up-conversion processes due to energy transfers between lanthanide ions.

Several fluoride glasses do not contain lanthanides in their starting compositions. Those are, for example, PZG glasses based on lead, zinc, and gallium fluorides, divalent fluoride glasses based on zinc, strontium, and barium fluorides (ZnSB), and chlorofluoride glasses based on cadmium chloride and fluoride (CNBK).[2−4] Depending on the ability of the glassy network to accommodate additional elements, rare earths can be incorporated in those materials up to a few percent or tenths of a percent. Rare-earth-doped PZG glasses were studied because they can form active films and waveguides by vapor phase deposition. On the other hand, divalent fluoride and chlorofluoride matrices are of fundamental interest because they exhibit low phonon energy and high emission efficiencies for lanthanide(III) ions.

The preparation of fluoride glasses obeys the classical steps of glass making, that is, mixing of the starting constituents, melting, cooling of the melt, and, finally, annealing of the glass before cutting and polishing. Ideally, fluoride glasses are synthesized from metal fluorides. However, due to the high cost or the unavailability of some fluorides, glass synthesis is also carried out from metal oxides. The action of a fluorinating agent such as the ammonium hydrogenodifluoride is then required to transform, for example, a lanthanide oxide into a fluoride. The chemical process is described by the following reaction:

$$Ln_2O_3 + 6NH_4F, HF \rightarrow 2(NH_4)_3 LnF_6 + 3H_2O\uparrow$$

with

$$(NH_4)_3 LnF_6 \rightarrow LnF_3 + 3NH_4F\uparrow \qquad (1)$$

The mixture of fluorides is melted in platinum or in a vitreous carbon crucible and heated to the refining temperature between 800 and 950 °C, depending on the glass composition. Because fluoride glasses are especially sensitive to atmospheric moisture in their liquid phase, melting must be carried out in a dry environment that can be neutral (N_2 or Ar) or reactive (NF_3 or SF_6). Reactive atmospheres are implemented to remove traces of hydroxyl ions from the glass. Then, the melt is cooled to a temperature close to the liquidus temperature and is poured in a brass mold preheated to the glass transition temperature, T_g. With thermally stable glasses such as ZBLAN, melts can be gently cooled in the crucible. Finally, the glass samples are annealed at a temperature close to T_g to relax the mechanical stresses that appear upon solidification.

Table 1. Chemical Composition of Lanthanide-Containing Fluoride Glasses

glass	composition
ZBLAN	$53ZrF_4{\cdot}20BaF_2{\cdot}4LaF_3{\cdot}3AlF_3{\cdot}20NaF$
BIG	$25BaF_2{\cdot}23InF_3{\cdot}12GaF_3{\cdot}25ZnF_2{\cdot}15GdF_3$

The technique most appropriate for synthesizing ultra-high-quality fluoride glasses is the levitation technique. Melting and cooling are carried out on a sustaining gas film. Thus, glass contamination by particles from crucibles and molds is absent, which results in glasses with low scattering losses. A Rayleigh scattering coefficient of 0.66 dB km^{-1} μm^4 was measured for a levitated ZBLAN fluoride glass, which is similar to that of silica glass.[5]

2. Physical Properties

The physical properties of some fluoride glasses are given in Table 2. Due to the relative weakness of M−F bonds, the characteristic temperatures of fluoride glasses are low, as compared to oxides. Thus, glass transition temperatures, T_g, of fluoride glasses are typically in the 300 °C range, and melting occurs at temperatures T_m between 450 and 600 °C, depending on the glass composition. An estimation of the glass stability is given by the Hruby factor: $H_r = (T_x - T_g/T_m - T_x)$, where T_x is the crystallization temperature, which must be as large as possible. On this basis, ZBLAN is very stable against devitrification. In addition, thermal analysis curves show a weak crystallization peak for that glass. These favorable conditions are confirmed experimentally by a better ability of ZBLAN for fiber drawing, as compared to other fluoride glasses. The densities (d), refractive indices at the sodium D-line (n_D), and linear expansion coefficients (α) are also given in Table 2.

Table 2. Physical Properties of Lanthanide-Containing Fluoride Glasses

glass	T_g (°C)	T_x (°C)	T_m (°C)	n_D	$\alpha(10^{-7}\ K^{-1})$
ZBLAN	262	352	455	1.498	200
BIG	324	469		1.505	170

Optical transmission is an essential physical characteristic of halide glasses in the sense that this property differentiates easily halide glasses from traditional oxide glasses. Fluoride glasses usually start transmitting at ~250 nm in the UV, which corresponds to an energy gap of ≈5 eV. For comparison, pure silica shows a better UV transparency with

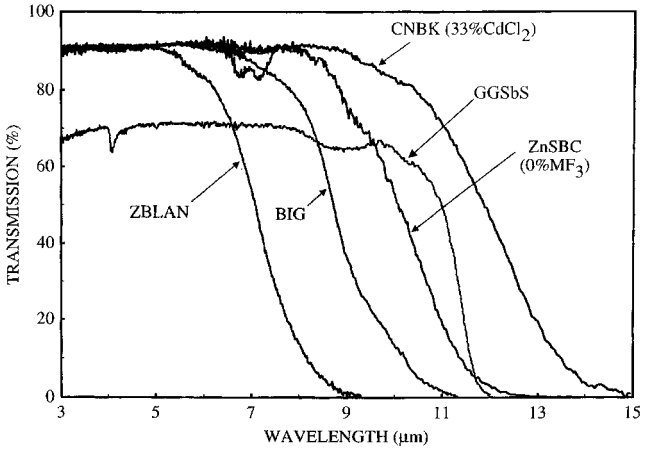

Figure 1. Infrared transmission spectra of non-oxide glasses. Acronyms are given in the text. M = trivalent metal ions.

an energy gap of ≈8 eV ($\lambda \approx 160$ nm). Infrared transmission spectra are shown in Figure 1 for typical fluoride glasses. Glasses with large, heavy, and lightly charged elements possess lower phonon energies and a consequent extended infrared transparency.

For ZBLAN, the IR edge is in the 5−8 μm range with a 50% transmission located at ≈7.1 μm (1400 cm^{-1}) for a 2-mm-thick sample. This is to be compared with silica glass, the transparency of which starts to decrease at ≈3 μm. The IR edge is due to multiphonon absorption processes related to the fundamental vibration frequencies of the host. For ZBLAN, Zr−F vibrations around 580 cm^{-1} account for the multiphonon absorption, whereas, for silica, the position of the IR edge is due to Si−O vibrations at 1100 cm^{-1}. A shift by >1.5 μm in the IR is observed for BIG fluoroindate glass as compared to standard ZBLAN glass.[6,7] This is due to the lower frequency of In−F bonds (≈510 cm^{-1}) with respect to Zr−F. The IR multiphonon edge may attain 10 μm at 50% maximum transmission for ZnF_2-based glasses, as shown in Figure 1 for ZnSBC (Zn−Sr−Ba−Cd) glass.[3] Partial substitution of fluoride ions by chlorides in CNBK glass results in an additional shift by nearly 2 μm in the infrared.[4]

3. Structural Environment of Lanthanides in Fluoride Glasses

In fluorozirconate and fluoroindate glasses, the formation of which is strongly improved by the presence of lanthanides, the rare-earth ions occupy glass former sites. This is supported by the profile of the emission spectra of lanthanides, which have similar full-width at half-maximum (fwhm) values in fluoride glass and crystals, indicating that lanthanide ions occupy well-defined sites in the glass.[8]

Several studies have been performed with fluoride glasses containing Eu^{3+} as probe ions for structural investigations. Site-selective spectroscopy has been carried out in fluorozirconate and chlorofluorozirconate.[9−11] The $^5D_0$ emitting level of europium is a singlet, and, therefore, the interpretation of band profiles is more straightforward than for transitions between multiplets. Thus, the measurements were carried out by monitoring the $^5D_0 \rightarrow {}^7F_1$ and the $^5D_0 \rightarrow {}^7F_2$ emissions under resonant excitation. All measurements show a similar spectral evolution, that is, a broadening of $^5D_0 \rightarrow {}^7F_1$ with decreasing excitation wavelength, which reflects the variety of sites in glasses. Moreover, additional components show up in the $^5D_0 \rightarrow {}^7F_1$ profile when excitation is in the high-energy side of the $^7F_0 \rightarrow {}^5D_0$ absorption band. Deconvolution of the spectra shows that six components are present, whereas only three Stark components are expected for $^5D_0 \rightarrow {}^7F_1$. A controversy exists about the interpretation of these six-component spectra. Some teams explain the occurrence of six components as being due to two nonequivalent types of sites connected by energy transfer as revealed by time-resolved spectroscopy.[9,11,12] Others consider that the six-component profile is the result of the superposition of emission from one type of site only and emission from the whole distribution of sites excited via the phonon-side band (PSB).[10,13] This approach, even though quite satisfactory, raises new questions such as the relatively narrow width of the $^5D_0 \rightarrow {}^7F_1$ transition via PSB excitation. PSB excitation, which is not selective, should lead to a broad emission spectrum due to the distribution of sites.

Spectroscopy of the $^5D_0$ level is also a valuable tool to investigate the point symmetry of Eu^{3+} ions in materials. It is well-known that the $^5D_0 \rightarrow {}^7F_2$ transition is electric-dipole in nature, whereas $^5D_0 \rightarrow {}^7F_1$ shows a magnetic-dipole character. $^5D_0 \rightarrow {}^7F_2$ is totally forbidden in the presence of an inversion center, and it is allowed in the opposite case. Usually, in vitreous phases, where the symmetry is low, electric dipolar transitions exhibit the strongest intensity. Fluorescence spectra show that both transitions have about the same intensity, indicating that Eu^{3+} ions are in high-symmetry sites in fluorozirconate glasses, relative to oxide glasses. Comparison of glass and crystal spectra suggests, in addition, that the site symmetry in fluorozirconates will be close to the 8-coordinate bicapped trigonal prism found in $EuZrF_7$. The similarity is confirmed with lifetime measurements[9] and by measurements of photoluminescence of devitrified samples.[13] The preferential coordination number of 8 is also confirmed by molecular dynamics simulation.[10]

III. Lanthanide-Containing Chalcogenide Glasses

1. Chemical Composition and Glass Synthesis

The most famous lanthanide-containing chalcogenide glass is made of gallium, lanthanum, and sulfur and is referred to as GaLaS or GLS in the literature. Its composition is given in Table 3. With 30% lanthanum sulfide, GLS can be doped with large

Table 3. Chemical Composition of Chalcogenide Glasses as Hosts for Lanthanide Elements

glass	composition
GLS	$70Ga_2S_3{\cdot}30La_2S_3$
GNS	$66Ga_2S_3{\cdot}34Na_2S$
GGSbS	$Ge_{20}Ga_5Sb_{10}S_{65}$
BIGGSe	$Ba_{32.5}In_{12.5}Ga_{12.5}Ge_{55}Se_{180}$
GGSe	$Ge_{30}Ga_5Se_{65}$

amounts of active rare-earth ions. Other chalcogenide glasses such as Ga−Na−S and Ge−Ga−Sb−S glasses accept only low concentrations of rare-earth ions, typically in the 1% range.

Selenium-based glasses are also susceptible to inclusion of rare-earth ions. Stable glass compositions are found in the Ge−Ga−Se ternary system.[14] Partial substitution of As for Ge leads to glasses suitable for fiber drawing.[15] Up to 1 cat. % lanthanide ions can be incorporated in selenium-based glasses.

Sulfide and selenide glasses are synthesized usually from single chemical elements. The final optical quality of the material depends strongly on the absence of any impurity, especially hydrogen and oxygen-based entities. Then, it is of prime importance that starting products be of ultrahigh chemical purity, 5 N at least. Additional treatments such as the distillation of sulfur and the deoxidation of the glass are needed for the preparation of optical fibers with low optical losses.

Weighed in a dry glovebox, the products are placed in a silica ampule, which is then pumped down to 10^{-4} Torr and sealed. To reduce as much as possible the contamination during synthesis, the walls of the silica ampule are primarily treated by a $HCl + HNO_3$ mixture, then rinsed with HF and deionized water, and finally dried with an oxyacetylene torch.

The sealed ampule is then placed in a rocking furnace. The heating rate has to be low, typically 1 °C min^{-1}, to avoid any explosion due to overpressure of unreacted gaseous sulfur. The synthesis temperature is typically in the 800−1000 °C range for GGSbS glasses. Lanthanide-containing chalcogenide glasses, such as GLS, are usually synthesized at higher temperatures close to 1200 °C. The melt is homogenized by rocking the furnace during ∼10 h. It is then quenched and annealed at the glass transition temperature, before being cooled to room temperature.

2. Physical Properties

The physical properties of some sulfide and selenide glasses are given in Table 4. Based on gallium sulfide, GLS and GNS glasses show high characteristic temperatures, as compared to fluorides, with T_g values of 556 and 484 °C, and T_x values of 830 and 720 °C, respectively. More properties, especially mechanical properties, can be found in ref 16. One should note the high thermal stability of GGSbS glass that exhibits not only a large $T_x - T_g$ temperature difference of 190 °C but also a very low crystallization peak.[17] Thermal stability is sufficiently high to allow fiber drawing with GLS, GNS, and GGSbS sulfide glass.

Table 4. Physical Properties of Chalcogenide Glasses as Hosts for Lanthanide Elements

glass	T_g (°C)	T_x (°C)	T_m (°C)	n	$\alpha(10^{-7}$ $K^{-1})$
GLS	556	681	830	≈2.48[a]	90
GNS	484	599	720		145
GGSSb	305	494		2.3657[b]	162
BIGGSe[c]	385	525			
GGSe	360				

[a] Refractive index measured at 589 nm. [b] Refractive index measured at 632.8 nm. [c] Pr^{3+}-doped glass.

Among the selenide glasses that accept rare-earth ions, let us mention BIGGSe, the glass transition temperature of which is located at 385 °C, that is, 140 °C below crystallization.

Because of the high polarizability of S^{2-} and Se^{2-} ions, as compared with the halides, the refractive indices of chalcogenide glasses are high, between 2 and 3, as shown in Table 4. Monitoring the glass composition can control values of the refractive indices. Thus, substitution of gallium sulfide for a few percent lanthanum sulfide results in an increase of the refractive index, so that core/clad structures with appropriate optical guiding properties can be realized. Partial S/Se substitution is another efficient method for tailoring refractive indices of chalcogenide glasses, as well as the modification of antimony(III) content, whenever possible. Thus, a refractive index as low as 2.241 was measured with 4% antimony in GGSbS glass, as compared with 2.365 for the glass with 10% Sb.[18]

The optical transmission spectrum of GGSbS is shown in Figure 1, with the infrared edge located at 10−11 μm. High Fresnel losses are responsible for the maximum transmission of 70%. The feature at 4 μm is due to the presence of S−H impurities, and that at 9 μm is attributed to a harmonic of a fundamental vibration mode of the matrix.

3. Structural Environment of Lanthanides in Chalcogenide Glasses

Investigations on the local environment of lanthanides in chalcogenide glasses are sparse in the literature. One reason is the difficulty of defining a coordination polyhedron for Ln elements with reliable methods.[19] However, EXAFS measurements carried out with GLS chalcogenide glasses modified by CsCl lead to some valuable information.[20] It should be remembered that, from the viewpoint of optical properties, the interest for CsCl is to shift the glass band gap toward shorter wavelengths, in the 500 nm range. Measurements performed at the chlorine K-edge show that Cl is essentially linked to Cs atoms. There is no significant occurrence of Ga−Cl bonding. This suggests that addition of chlorine results essentially in modifications of the lanthanum environment. Spectroscopic measurements of GeGaS−CsCl glass doped with Nd^{3+} confirm that lanthanides are preferentially surrounded by chloride atoms in this type of glass.[21] Absorption transitions of lanthanides are red-shifted in a covalent environment, as compared to an ionic environment. Known as the nephelauxetic effect, the phenomenon is observed in covalent GGS−CsI glasses, as shown in Figure 2. This is a direct indication of the dominant ionic nature of the lanthanide environment in GGS−CsCl. On the other hand, chloride atoms bond preferentially to lanthanides. The low absorption coefficient of the $^4I_{9/2} \rightarrow (^4G_{5/2}, {}^2G_{7/2})$ transition confirms the ionic character of the lanthanide environment in GGS−Cl glass.

Structural investigations by Shin et al. and Tverjanovich et al. have shown that $(GaS_{3/2}X)^-$ and units were present in GGS−MX glasses (M = alkali; X = halogen).[22,23] Then, a reasonable hypothesis is that

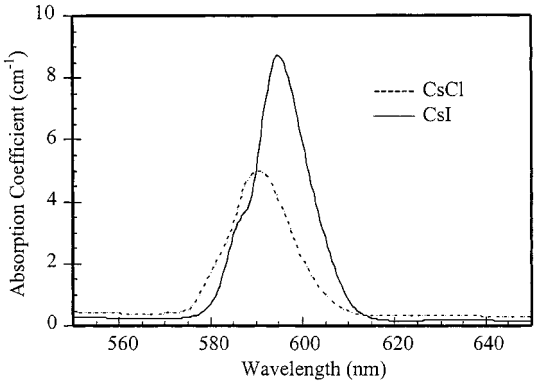

Figure 2. Nephelauxetic effect in the absorption spectrum of Nd^{3+} ($^4I_{9/2} \rightarrow {}^4G_{5/2}$, $^2G_{7/2}$ transition) in GGS−CsI and GGS−CsCl sulfide glass.

$(GaS_{3/2}Cl)^-$ units surround the lanthanide ions in GGS−CsCl glasses.

IV. Optical Properties of Lanthanide(III) Ions in Non-Oxide Glasses

Non-oxide glasses are hosts of prime interest for rare-earth spectroscopy. They show low phonon energies, which induce high quantum efficiencies of rare-earth emissions. Thus, a number of transitions, which cannot be detected in silica-based rare-earth-doped glasses, are observed in non-oxide glasses.

1. General Properties

The radiative and nonradiative properties of lanthanide(III) ions have been widely reported. Especially, the Judd−Ofelt theory has been applied to most rare-earth−fluoride-glass combinations. Typical Judd−Ofelt parameters are reported in Table 5 for ZBLAN glass.[24−26] An exhaustive list of such parameters for glasses and crystals can be found in ref 27.

Table 5. Judd−Ofelt Parameters Ω_t (t = 2, 4, and 6, in 10^{-20} cm^2 Units) of Lanthanide Ions in ZBLAN Fluoride Glass

rare-earth ion	Ω_2	Ω_4	Ω_6	ref
Pr^{3+}	1.60	5.06	4.79	24
Nd^{3+}	2.20	2.82	3.94	24
Sm^{3+}	2.06	2.55	1.63	25
Eu^{3+}	2.89	3.87	2.88	27
Gd^{3+}	3.35		2.81	26
Tb^{3+}	0.03	1.88	2.48	25
Dy^{3+}	3.03	1.32	2.06	25
Ho^{3+}	2.14	2.22	2.05	27
Er^{3+}	2.67	1.41	1.02	24
Tm^{3+}	2.21	1.71	0.92	25

In most cases, the Judd−Ofelt parameters are calculated with good confidence in fluoride glasses, as suggested by the convergence of results obtained by various laboratories. They are found to adequately predict the radiative properties—lifetimes and branching ratios—of several transitions especially for Ho^{3+}, Er^{3+}, and Tm^{3+} ions in ZBLAN as well as in fluoroindate glasses.

Conversely, the Judd−Ofelt approach is not satisfactory for Pr^{3+} ions in fluoride glasses. This is actually a problem observed in most optical hosts, due to a mixing effect between the 4f and 5d electrons of praseodymium. In addition, in most cases, the strong hypersensitive $^3P_2$ absorption band has to be suppressed from the fitting procedure to obtain a positive Ω_2 parameter. For ZBLAN, the Judd−Ofelt parametrization is found to fairly predict the radiative lifetime and branching ratios for the $^3P_0$ emitting level, whereas only branching ratios can be evaluated for $^1D_2$. Depending on the authors, the computed radiative lifetime of the $^1G_4$ level is given between 2 and 3.8 ms.

Several modified Judd−Ofelt theories were proposed to better account for the optical properties of Pr^{3+}. Thus, a four-phenomenological-parameter procedure leads to a significant improvement of the quality of the fit and a consequent acceptable agreement between experimental and calculated lifetimes for the $^1D_2$ level.[28] Other techniques incorporate the measured fluorescence branching ratios[29] or take into account a relative deviation between experimental and calculated oscillator strengths.[30]

Determining the Judd−Ofelt parameters in sulfide and selenide glasses is a challenge. The position of the band gap located in the red or in the IR limits dramatically the number of absorption bands available for performing the Judd−Ofelt calculation. As a result, the parameters are determined with less confidence. However, even with this higher degree of uncertainty, Judd−Ofelt parameters remain of practical interest because they are very often the only solution for determining the radiative properties of lanthanide(III) ions.

Table 6 lists the Judd−Ofelt parameters of lanthanide(III) ions in various chalcogenide glasses, either sulfides or selenides.[17,21,31−39] Whatever the lanthanide, Ω_2 parameters are large in chalcogenide glasses, as compared to fluorides. This is due to the covalent nature of chemical bondings around the rare-earth ion. When CsCl is added to GGS sulfide glass, the Ω_2 parameter of Nd^{3+} decreases, compared to the CsI-containing glass. This result is in accordance with the probable surrounding of lanthanides by chloride ions in sulfohalide glasses, as mentioned before. In the Pr^{3+} series, the highest Ω_2 parameter is obtained for a selenide glass, the covalent nature of which overpasses that of sulfides.

The validity of the Judd−Ofelt treatment is questionable for chalcogenide glasses, especially for Tm^{3+}, which shows only four absorption bands within the transmission domain of sulfide glasses. Despite these

Table 6. Judd−Ofelt Parameters Ω_t (t = 2, 4, and 6, in 10^{-20} cm^2 Units) of Lanthanide Ions in Sulfide and Selenide Glasses

rare-earth ion	glass	Ω_2	Ω_4	Ω_6	ref
Pr^{3+}	GLS	6.9	5.5	1.07	31
	GeAsS	6.98	2.53	0.78	32
	BaInGaGe−Se	15.7	4.0	12.7	33
Nd^{3+}	GLS	7.7	7.65	4.86	34
	GGS−CsI	11.3	11.3	7.58	21
	GGS−CsCl	7.09	8.99	5.03	21
Dy^{3+}	GLS	11.3	1.0	1.3	35
	GGSbS	9.49	2.29	1.79	17
Er^{3+}	GLS	6.54	2.00	0.97	36
Tm^{3+}	GGSbS	6.7	2.0	2.6	37
	GGLS	7.11	1.46	1.95	38
	GeAsS	5.67	1.74	1.82	39

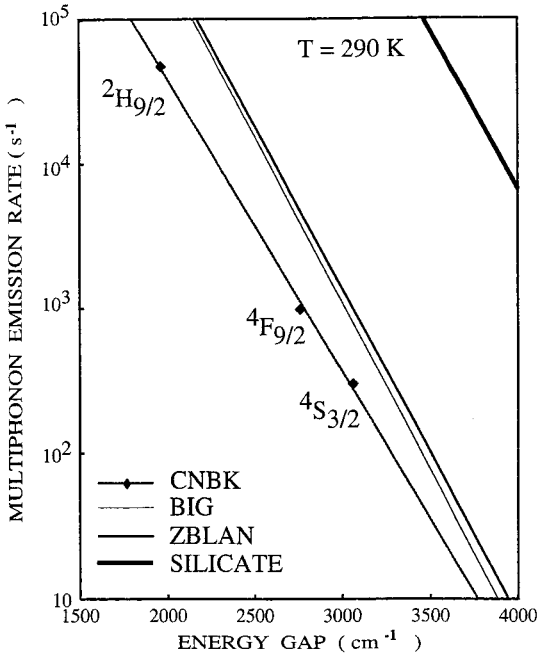

Figure 3. Multiphonon emission rates of rare-earth ions in silicate, fluoride, and chlorofluoride glasses. The positions of three levels of Er^{3+} ions are indicated, with respect to the energy gap to the next lower level.

poor conditions for applying the theory, the Ω parameters predict with very good accuracy the $^3H_4$ lifetime (≈120 μs) of Tm^{3+} in GGSbS glass. On the contrary, the lifetime for the $^3F_4$ level is largely underestimated.[37] With six or more transitions involved, results are more reliable for Pr^{3+}, Nd^{3+}, and Dy^{3+}.

One of the main spectroscopic properties that differentiate non-oxide glasses from silica-based glasses is the low multiphonon emission rate. These nonradiative relaxations, which may strongly compete with radiative processes in rare-earth ions, are nearly 3 orders of magnitude lower in ZBLAN glass than in silicate, as shown in Figure 3. This property is directly related to the fundamental vibration modes of the host and, therefore, varies basically in the same manner as the infrared absorption edge.

Raman spectroscopy or far-IR spectroscopy can determine the fundamental vibration frequencies of the host. However, these methods give information about the whole glass matrix and do not account for the local nature of electron−phonon interactions. Therefore, the fundamental frequencies are preferably determined by recording the phonon side bands (PSB) of rare-earth transitions or by studying the temperature dependence of multiphonon relaxations.[40,41] The phonon energies determined by PSB spectroscopy, which is the most direct method, are usually lower (400 cm^{-1} in ZBLAN) than those measured by other methods (≈500 cm^{-1}), suggesting that weak M−F bonds are effectively coupled to the rare earth.[41] In cadmium chlorofluoride glass (CNBK), the highest phonon energy is ∼370 cm^{-1}, which corresponds to Cd−F vibrations.[42] This results in low multiphonon emission rates for that glass, as shown in Figure 3.

In GGSbS sulfide glasses, the fundamental vibration modes are equal to 340 cm^{-1}, as shown in Figure

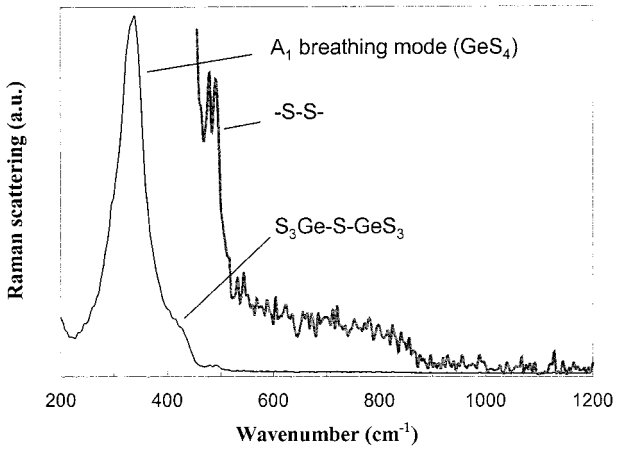

Figure 4. Raman spectrum of GGSbS sulfide glass.

4. They correspond to the "breathing mode" of GeS_4 tetrahedra that form the glass network. The shoulder located at 430 cm^{-1} is attributed to $S_3Ge-S-GeS_3$ vibration modes, whereas the structure observed at 470 cm^{-1} is due to the presence of −S−S− bonds, the glass composition being nonstoichiometric. The weak band in the 600−800 cm^{-1} region is explained by the presence of residual oxygen within the glass, leading to the formation of high-frequency M−O vibrations. In selenide glasses such as GGSe, the dominant vibration mode measured by Raman spectroscopy is located at 200 cm^{-1}. Several secondary modes between 210 and 310 cm^{-1} are also observed.[43] Just as in sulfides, the dominant mode is due to the symmetric breathing mode of the glass-forming tetrahedra, namely, $GeSe_4$ in selenides.

2. Praseodymium (Pr^{3+})

The optical properties of Pr^{3+} ions have been studied in various fluoride glasses based on zirconium,[44,45] indium,[46,47] or zinc fluorides.[46,48]

Pr^{3+}-doped fluoride glasses are efficient emitters in the visible with strong emissions in the blue, green, and red domains from the ($^3P_0$, $^3P_1$) levels as shown in Figure 5. These levels can be excited by various up-conversion mechanisms, that is, with light at 588 nm into the $^1D_2$ level followed by a cross-relaxation or by means of two-step excited state absorption (ESA) mechanisms involving two different wavelengths.[49,50]

The 1.3 μm emission of Pr^{3+} ions has been extensively studied because of its suitability for optical amplification in the fiber telecommunication technology. This emission, which occurs from the $^1G_4$ excited state to the $^3H_5$ level, peaks at 1.31 μm. Because of an energy gap of ∼3000 cm^{-1} between $^1G_4$ and $^3F_4$, this transition is observed exclusively in low-phonon-energy materials such as fluorides, chlorides, and sulfides. It shows a favorable branching ratio of nearly 0.65 in fluoride glasses,[24] and ESA of the emission wavelength, located in the long-wavelength side of the band,[51] is by far not as severe as for the 1.3 μm emission of Nd^{3+} ions. A main drawback is the weak oscillator strength of the $^3H_4 \rightarrow {}^1G_4$ absorption, which results in poor pumping conditions. This can be improved by codoping with Yb^{3+}, which has a $^2F_{5/2}$ level coinciding with $^1G_4$.[52]

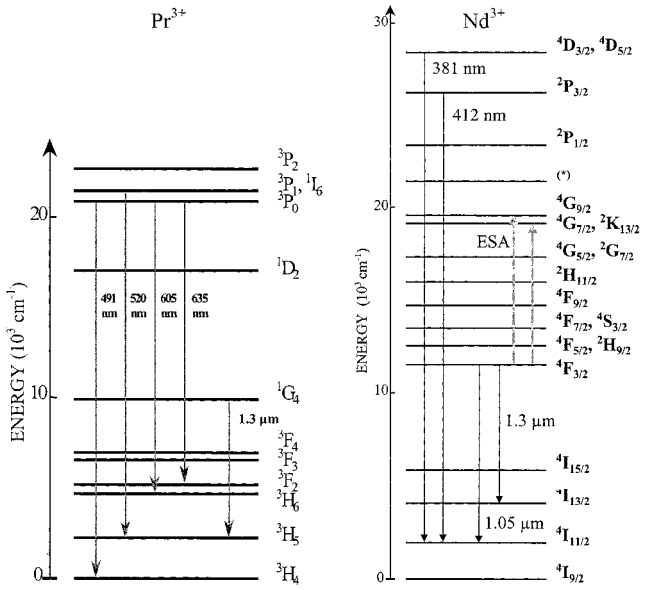

Figure 5. Energy level diagram and selected transitions of Pr^{3+} and Nd^{3+} ions in non-oxide glasses. (*) $^2D_{3/2}$, $^2G_{9/2}$, $^4G_{11/2}$, and $^2K_{15/2}$ levels of Nd^{3+}.

Researchers at Corning Inc. have demonstrated 1.3 μm emission in a Pr^{3+}-doped oxyfluoride glass ceramic.[53] A relatively high quantum efficiency of 8−9% was found, to be compared with 3% in ZBLAN glass. This indicates that Pr^{3+} ions are embedded in a crystalline fluoride environment. With such oxyfluoride vitroceramics, one takes advantage of the good mechanical properties of oxide materials, of easier shaping of glasses and better emission efficiencies of lanthanides in the crystallized fluoride environment. Recently, an efficient neodymium-doped glass−ceramic fiber laser operating at 1.05 μm was demonstrated.[54] The fiber was made of aluminosilicate glass containing cadmium, lead, and yttrium fluorides. X-ray and electron microscopic data performed on bulk materials indicate that the crystal size is ≤10 nm in diameter.

Praseodymium(III) ions have been introduced in sulfide and selenide glasses as well, with the aim to increase the quantum efficiency of the 1.3 μm emission. Thus, quantum efficiencies as high as 58% were determined for the 1.3 μm emission in GLS and GNS glass.[55] The lifetime, τ, of the $^1G_4$ emitting level is typically in the 300 μs range, to be compared with 110 μs in ZBLAN fluoride glass. Combined with the large emission cross sections, σ, inherent in chalcogenide matrices, such increased lifetimes result in high gain coefficients in sulfides (see section V.2).

Infrared to visible up-conversion processes have been studied for Pr^{3+} ions in GGS−CsX glasses (X = Cl, Br, and I).[56] Because of the extended transmission domain of these sulfide glasses, transitions from the upper $^3P_0$ level could be observed. With excitation at 1020 nm from a Ti:sapphire laser, emission from the $^1D_2$ level is dominant. The mechanism involved is direct excitation of the $^1G_4$ level followed by energy transfer up-conversion ($^1G_4$, $^1G_4 \rightarrow {}^1D_2$, $^3H_5$). With 979 nm excitation, that is, at higher energy, slightly above the $^1G_4$ level, then transitions from the $^3P_0$ level are the most intense. In that case, an excited state absorption (ESA) of the pump wavelength accounts for the excitation of the $^3P_0$ level.

Several transitions that cannot be observed in fluoride glasses were detected in rare-earth-doped chalcogenides, especially at wavelengths >2 μm. Thus, emissions at 3.4 μm and in the 4−5 μm range were recorded in a Ba−In−Ga−Ge selenide glass doped with Pr^{3+}.[33] These emissions are attributed to transitions from the ($^3F_4$, $^3F_3$), ($^3F_2$, $^3H_6$), and $^3H_5$ levels. Emissions from ($^3F_2$, $^3H_6$) and $^3H_5$ were also observed in a core/clad selenium glass fiber containing praseodymium.[15]

3. Neodymium (Nd^{3+})

Nd^{3+} ions are by far the most widely investigated ions in all types of materials, essentially because of the ideal, four-level, 1.06 μm laser transition from $^4F_{3/2}$ to $^4I_{11/2}$. Thus, the spectroscopic properties of Nd^{3+} ions are reported for a large number of different compositions of fluoride and chalcogenide glasses.[24,57−61]

Due to the low phonon energy of fluoride glasses, some high energy levels of Nd^{3+} ions can be efficiently populated, leading to emissions at several wavelengths ranging from the UV to the red. These emitting high-energy levels are indicated in the diagram in Figure 5 with the two most intense transitions, $^4D_{3/2} \rightarrow {}^4I_{11/2}$ at 381 nm and $^2P_{3/2} \rightarrow {}^4I_{11/2}$ at 412 nm. Up-conversion processes involving two photons of 532 nm from a doubled Nd:YAG laser can pump these levels.

Up-converted UV and visible emissions occur also from lower lying levels such as $^2P_{1/2}$, ($^2D_{3/2}$, $^2G_{9/2}$, $^4G_{11/2}$, $^2K_{15/2}$), $^4G_{7/2}$, and $^4G_{5/2}$ with excitation at 532 or 801 nm.[62,63] Excitation of $^4D_{3/2}$ requires a three-step process with 801 nm pumping. Due to the predominance of multiphonon relaxations from these levels, experimental lifetimes are very short, in the tens of nanoseconds range.

Infrared to visible up-conversion processes have been studied for Nd^{3+} ions in GGS−CsX sulfide glasses (X = Cl, Br, and I).[61] With resonant excitation of the $^4F_{3/2}$ level at 888 nm, emission lines are observed from the $^4G_{7/2}$ level only. The mechanism involved is direct excitation of $^4F_{3/2}$ followed by energy transfer up-conversion ($^4F_{3/2}$, $^4F_{3/2} \rightarrow {}^4G_{7/2}$, $^4I_{7/2}$). With high energy excitation at 818 nm, into the ($^4F_{5/2}$, $^2H_{9/2}$) levels, then a transition at 438 nm from the ($^2P_{1/2}$, $^2D_{5/2}$) level appears in the spectrum. In that case, an excited state absorption of the pump wavelength accounts for the excitation of the ($^2P_{1/2}$, $^2D_{5/2}$) levels.

With an emission at 1.3 μm, Nd^{3+} is a potential candidate for optical amplification in the second telecommunication window. However, optical gain remains limited because of amplified spontaneous emission at 1.05 μm and also because of strong ESA at 1.3 μm. This ESA process, which takes place from $^4F_{3/2}$ to ($^4G_{7/2}$, $^2K_{13/2}$) and to $^4G_{9/2}$ as shown in Figure 5, is so probable that no gain is achieved around 1.3 μm in silica fibers. In ZBLAN fluoride fibers, gain is achieved at 1.34 μm. A pump−probe technique was developed to investigate ESA processes with bulk samples, with no measurements on optical fibers, the preparation of which is more difficult and time-

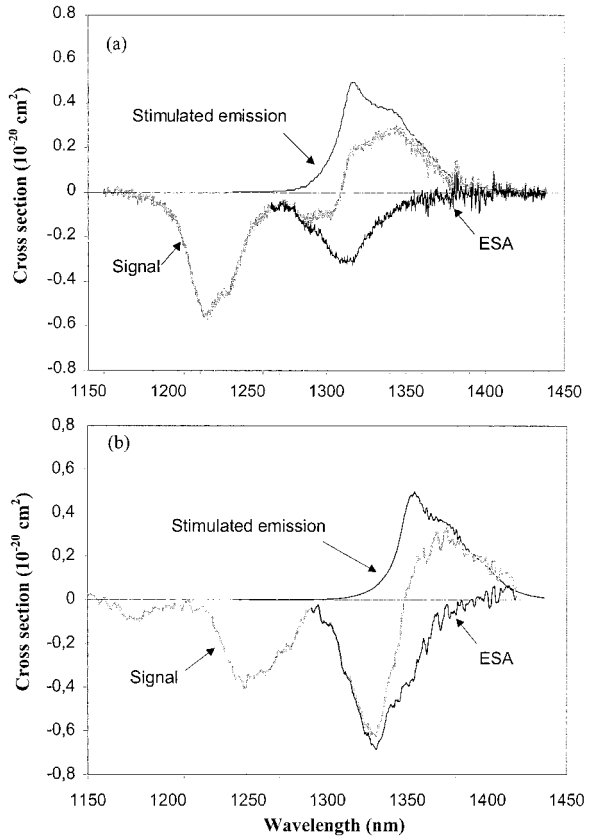

Figure 6. Excited state absorption in the 1.3 μm region in ZBLAN (a) and GGSbS:Nd^{3+} (b) glass.

consuming. The gain and ESA profiles determined by this technique for ZBLAN and GGSbS bulk glasses are shown in Figure 6 .[64] The results confirm that gain can be obtained in the 1.34 μm range in ZBLAN. They show that in GGSbS sulfide glasses, the situation is more dramatic, with low gain to be expected around 1.37 μm.

4. Dysprosium (Dy^{3+})

The Judd−Ofelt parameters, radiative properties, and emission spectra of Dy^{3+} ions have been investigated in several fluoride glasses, namely, fluorozirconates, PZG, fluorozincate, and fluoroindate glasses.[65−68] Excitation in the UV results in visible emissions from the $^4F_{9/2}$ level. One of the main interests of Dy^{3+} ions is the 1.3 μm emission from ($^6F_{11/2}$ + $^6H_{9/2}$) to the ground state, which could be utilized for optical amplification in the XS-band in telecommunication. However, with an energy gap to the next lower level of 1900 cm^{-1}, this group of levels cannot emit in any of the glasses listed above. Four phonons only are required for spanning the energy gap, which makes the multiphonon relaxation very probable. In sulfide glasses, which have phonon energies of ∼350 cm^{-1}, the 1.3 μm emission of Dy^{3+} is observed.[17] Further in the infrared, transitions at 1.8, 2.9, and 4.3 μm are measured in sulfide glasses, as well as in selenides.[69,14] They originate from the $^6H_{11/2}$ and $^6H_{13/2}$ levels.

5. Holmium (Ho^{3+})

Due to its numerous radiative emissions in the visible and the IR, holmium has been extensively studied in various fluoride glasses.[70−72] Several transitions are of special interest, namely, ($^5S_2$, $^5F_4$) → $^5I_8$ around 540 nm, $^5I_7$ → $^5I_8$ at 2 μm, and $^5I_5$ → $^5I_6$ at 3.9 μm. These transitions are shown in the energy level diagram in Figure 7. Emission in the visible can be obtained with excitation in the IR, via up-conversion processes. Thus, blue and green emissions are observed with excitation at 647 nm in Ho^{3+} singly doped fluorozirconate and fluoroaluminate glasses.[73,74] The process involves two photons according to the following pumping schemes: ($^5I_8$ → $^5F_5$) + ($^5I_6$ → $^5G_5$ and $^5I_7$ → $^5F_3$). The populations of the intermediate levels, $^5I_6$ and $^5I_7$, dominate the up-conversion efficiency.

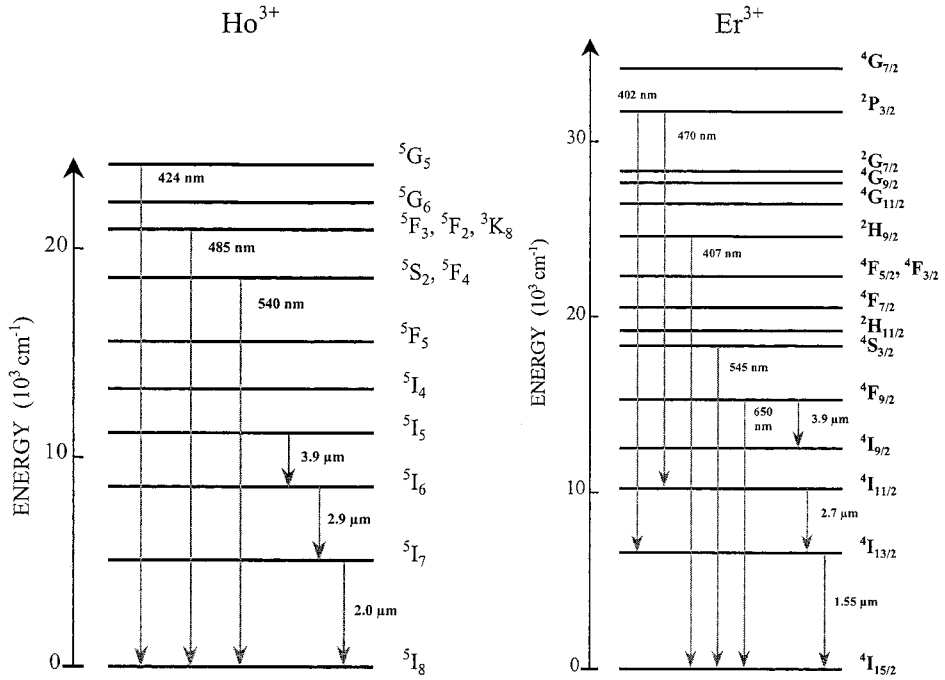

Figure 7. Energy level diagram and selected emissions of Ho^{3+} and Er^{3+} ions in non-oxide glasses.

The green emission from $^5S_2$ can also be observed in (Yb, Ho) codoped glasses.[75] This is due to a two-step energy-transfer up-conversion mechanism with excitation around 980 nm, that is, in the strong $^2F_{7/2} \rightarrow {}^2F_{5/2}$ absorption band of Yb^{3+} ions. The first transfer from Yb^{3+} to Ho^{3+} ($^5I_6$) is nonresonant, necessitating the dissipation of an energy of ~1600 cm^{-1} in the lattice. The second transfer promotes the electrons from $^5I_6$ to $^5S_2$.

The 2 μm emission from $^5I_7$ to $^5I_8$ was observed in bulk Ho^{3+}−fluoride glasses. This transition could be enhanced by appropriate codoping with Yb^{3+} or (Er^{3+}, Tm^{3+}).[76] The 3.9 μm transition shows a very weak branching ratio and quantum efficiency, so that it is observed only at liquid nitrogen temperature, in fiber configuration. More details are given in section V.1.

In sulfide glasses, holmium(III) ions emit at numerous wavelengths in the infrared because of the low phonon energy of the host. Especially, emissions are observed at room temperature in GLS glass from the $^5I_5$ levels at 1.67 μm and 3.9 μm and from $^5I_4$ at 1.25, 2.2, and 4.9 μm.[31] Despite a quantum efficiency of 1%, the 4.9 μm transition could find application in gas sensors because it corresponds to the absorption band of carbon monoxide.

6. Erbium (Er^{3+})

Erbium ions in fluoride glasses possess several radiative transitions from the violet to the mid-IR (3.45 μm) as shown in Figure 7. Their spectroscopic parameters such as radiative lifetimes and branching ratios were determined for several types of glasses based on zirconium, indium, aluminum, or even zinc fluoride.[24,77,78]

High-energy levels can be pumped efficiently by up-conversion processes. Thus, Takahashi et al. showed that a strong green emission from $^4S_{3/2}$ and a red emission from $^4F_{3/2}$ could be observed in an Er^{3+}-doped fluorozirconate glass with excitation at 800 nm, into $^4I_{9/2}$.[79] The mechanism involved two photons via ($^4I_{15/2} \rightarrow {}^4I_{9/2}$) + ($^4I_{11/2} \rightarrow {}^4F_{3/2}$ and $^4I_{13/2} \rightarrow {}^4S_{3/2}$), the energy in excess being absorbed by the phonons of the host. More recently, green emission was also measured with excitation at 833 nm, that is, between the $^4I_{9/2}$ and $^4I_{11/2}$ levels, in a fluoroindogallate glass. The $^4S_{3/2}$ emitting level of Er^{3+} was populated by two-step avalanche processes combined with cross-relaxation mechanisms from the $^2H_{11/2}$ thermalized level.[80]

Whereas the green emission is essentially due to an ESA process, additional energy transfer governs the red emission, as suggested by the increase of the red to green intensity ratio with Er^{3+} concentration. Energy transfer is possible through several cross-relaxation mechanisms: ($^4S_{3/2} \rightarrow {}^4F_{9/2}$; $^4I_{9/2} \rightarrow {}^4F_{9/2}$), ($^4S_{3/2} \rightarrow {}^4I_{11/2}$; $^4I_{13/2} \rightarrow {}^4F_{9/2}$), and ($^4I_{9/2} \rightarrow {}^4I_{13/2}$; $^4I_{11/2} \rightarrow {}^4F_{9/2}$). Cho et al. have shown that Tm^{3+}-codoping results in a significant increase of up-conversion efficiencies with 786 nm pumping.[81] This is explained by three successive energy transfer steps involving the $^3H_4 \rightarrow {}^3F_4$ transition in Tm^{3+} and ($^4I_{15/2} \rightarrow {}^4I_{13/2}$, $^4I_{13/2} \rightarrow {}^4I_{9/2}$, $^4I_{9/2} \rightarrow {}^2H_{11/2}$) in Er^{3+}.

Pumping around 800 nm can also initiate three-step up-conversion mechanisms leading to violet emission at 407 nm from $^2H_{9/2}$.[82] The third step originates either from $^4F_{9/2}$ or from $^4I_{9/2}$.

The violet, green, and red emissions of Er^{3+} ions in fluoride glasses can also be obtained with excitation at 650 nm and 1.48 μm, which are other spectral domains where laser diodes are commercially available. Violet and green emissions are obtained through a two-step 650-nm up-conversion process, whereas four and three steps are required with 1.48 μm pumping.[83]

Three-fold up-conversion of 637 nm light results in excitation of the $^2P_{3/2}$ level via ($^4I_{15/2} \rightarrow {}^4F_{9/2}$) + ($^4I_{13/2} \rightarrow {}^4F_{5/2}$) + ($^4S_{3/2} \rightarrow {}^4G_{7/2}$), each step being followed by multiphonon relaxations. Efficient blue (470 nm) and violet (402 nm) emissions occur from that level together with weak UV emission at 320 nm down to the $^4I_{15/2}$ ground state.[84]

Two-fold energy-transfer up-conversion occurs in (Yb, Er) codoped fluoride glasses with excitation at 980 nm into Yb^{3+} ions. Energy transfer takes place from the $^2F_{5/2}$ level of a first Yb^{3+} ion to the quasi-resonant $^4I_{11/2}$ level of Er^{3+}. Then, transfer from a second Yb^{3+} ion promotes the electrons to $^4F_{7/2}$ (Er^{3+}) and, after successive multiphonon relaxations, green and red emissions from $^4S_{3/2}$ and $^4F_{9/2}$ are observed.[85]

Further in the infrared, lasing in the 2.7−2.8 μm was obtained with Er^{3+} in bulk fluorozirconate glasses.[86] Glass samples were slabs with a few millimeter thickness and high rare-earth concentration (5−8 mol %). Lasing was obtained for the first time with diode pumping at 970 nm. A record output of 164 mW was demonstrated with an incident pump power of 1.8 W.

The spectroscopy of Er^{3+} ions was investigated in sulfide glasses as well. Infrared fluorescence was recorded at 1.54 μm from the $^4I_{13/2}$ level and at 980 nm and 2.75 μm from $^4I_{11/2}$ in GLS and GGSbS glasses.[36,87] Compared to silica, the emission cross section at 1.54 μm is 2.5 times greater in GLS glass, because of the high refractive index and covalent nature of the host. Green and red emissions could be measured in a GeGaLa sulfide glass.[88] The emitting levels, ($^4S_{3/2}$, $^2H_{11/2}$) and $^4F_{3/2}$, were populated by up-conversion with 800 nm excitation.

7. Thulium (Tm^{3+})

Fundamental properties of Tm^{3+} ions, such as spontaneous emission probabilities and radiative lifetimes, have been established in fluorozirconate[89] and in fluoroindate[90] glasses. The emission spectrum of Tm^{3+} is especially rich, with transitions ranging from the UV to the IR as shown in the energy level diagram in Figure 8. One should note the blue emissions that occur from the $^1G_4$ and $^1D_2$ levels and the IR emission at 1.47 μm from $^3H_4$ to $^3F_4$ suitable for amplification in the S-telecommunication band. Ultraviolet and blue emissions are also reported from the high-energy $^1I_6$ level located at nearly 35000 cm^{-1} (not shown).

Tm^{3+} ions in fluoride glasses are capable of emitting strong blue light with excitation in the red, around 650 nm. The $^1D_2$ level is populated via the two-step ($^3H_6 \rightarrow {}^3F_2 + {}^3H_4 \rightarrow {}^1D_2$) up-conversion mechanism with intermediate nonradiative relax-

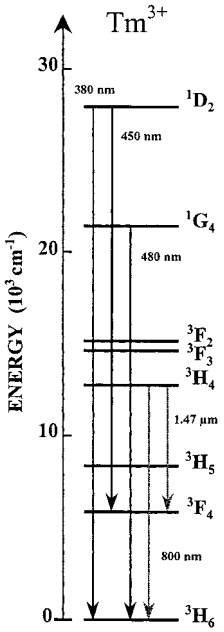

Figure 8. Energy level diagram and selected emissions of Tm^{3+} ions in non-oxide glasses.

ations from $^3F_2$ to $^3H_4$.[91] It must be noted that additional nonradiative and radiative decays occur from $^3H_4$ to the $^3F_4$ level, which has a lifetime long enough to permit absorption of a second 650 nm photon up to $^1G_4$. Thus, blue emission can also be obtained from that level by two-step up-conversion pumping.[92] The up-conversion fluorescence intensity is strongly host-dependent. It increases with decreasing phonon energy, that is, with longer fluorescence lifetimes of the intermediate levels, $^3H_4$ and $^3F_4$.

Similarly to Er^{3+} ions, Tm^{3+} ions in fluoride glasses are very efficiently excited by energy transfer from Yb^{3+} ions. Up-conversion processes have been demonstrated in various (Yb, Tm) codoped fluoride glasses.[93,94] Strong blue emissions from $^1D_2$ and $^1G_4$ are observed with excitation at 975 nm in a codoped fluoroindate glass. For low-power pumping, the $^1G_4 \rightarrow {}^3H_6$ transition at 480 nm is predominant. The upper level is populated by a three-step up-conversion. With higher pump powers, the $^1D_2 \rightarrow {}^3F_4$ transition at 450 nm increases dramatically. This phenomenon is interpreted as being due to a higher population of the $^3F_4$ level for high pump powers, resulting in excited state absorption of 480 nm light from $^1G_4$ and consequent excitation of the $^1D_2$ level.

The 800 nm transition from $^3H_4$ to $^3H_6$ has been extensively studied because of its suitability for optical amplification in the first telecommunication window, a spectral range where cheap sources and detectors are available. However, the 800 nm technology is not used for long-haul communication because of high optical losses of silica fibers in that window.

The $^3H_4 \rightarrow {}^3F_4$ transition of Tm^{3+}, around 1.47 μm, has been especially studied in fluoride and chalcogenide glasses. It was found that the emission band is similar in ZBLAN fluoride glass and in GGSbS sulfide glass, in terms of position (peak at 1.47 μm) and profile (fwhm $\approx$ 75 nm).[37] Interest in Tm^{3+} in sulfide glasses remains in the high absorption cross sections—5 times as high as in fluorides—that lead to better pumping conditions for optical amplification in the S-band (see section V.2).

V. Applications of Non-Oxide Glasses Containing Lanthanides

Most applications such as fiber lasers and optical amplifiers require that light be guided in the lanthanide-containing glasses. Thus, original techniques have been developed to make optical fibers from non-oxide glasses. Comprehensive information on such techniques is available in the literature.[95−97] Basically, single-mode fibers are pulled from preforms that are prepared by various methods: preform jacketing, rod-in-tube, extrusion, or double-crucible. The best results to date, in terms of optical attenuation, are 0.45 dB km^{-1} at 2.35 μm for 60 m ZBLAN single-mode fibers, that is, fibers with a core radius in the 2−10 μm range for an outside diameter of 150 μm. Optical losses approach 1 dB m^{-1} at 4 μm for a 2 m GLS sulfide fiber.[16,98] Losses are due typically to residual O−H and transition metal impurities with additional absorption due to S−H and Se−H groups in chalcogenide glasses. Consequently, the use of lanthanide-containing non-oxide glass fibers is limited to short- and medium-distance applications.

Research has been devoted to the development of planar waveguides, as well. Anionic exchange and physical vapor deposition were successfully implemented for the preparation of lanthanide-containing fluoride glass channel waveguides.[99,100]

1. Fiber Lasers

Although very few fluoride glass lasers exist in bulk configuration,[86,101] more than 30 lasers have been demonstrated in fiber configuration. The optical confinement inherent in optical fibers results in high-pump light density in the core of the fiber and, consequently, in large population inversion. In addition, the fiber geometry is adequate for releasing the heat generated by possible nonradiative processes concomitant to lasing. Optical confinement necessitates the use of single-mode optical fibers. The rare-earth concentration in the core of the fiber is typically 100−1000 ppm, possibly 1%. Usually, the length is from a few centimeters to several meters. Numerical apertures as large as 0.4 can be obtained with ZBLAN fluoride glass by addition of lead fluoride in the core and hafnium in the cladding.

The lasing wavelengths that have been observed with lanthanide-doped fluoride glass fibers are shown in Table 7. Each of them is characterized by the highest output power reported to date and by the pumping conditions, either direct or by means of up-conversion processes.[102−115]

The development of up-conversion fiber lasers, especially in the visible, is assisted by the availability of intense semiconductor lasers and minicrystal lasers for pump sources. The various energy levels involved in the transitions are detailed in the energy level diagrams of Figures 5, 7,and 8.

Room temperature lasing has been demonstrated in the ultraviolet at 381 nm and in the violet at 412

Table 7. Characteristics of Rare-Earth-Doped ZBLAN Fluoride Glass Fiber Lasers

λ (μm)	rare-earth	output power	pump characteristics[a]	ref
0.381	Nd	74 μW	590 nm (uc); 275 mW (i)	116
0.412	Nd	500 μW	590 nm (uc); 320 mW (i)	117
0.455	Tm	3 mW	(645 + 1064) nm (uc); (600 + 230) mW (i)	162
0.481	Tm	230 mW	1123 nm (uc); 1.6 W (i)	163
0.492	Pr	22 mw	(1017 + 835) nm (uc); (250 + 42) mW (l)	164
0.520	Pr	2 mW	476 nm; 500 mW (i)	165
0.546	Er	23 mW	801 nm (uc); 780 mW (a)	166
0.549	Ho	38 mW	643 nm (uc); 280 mW (a)	120
0.605	Pr	150 mW	476 nm; 800 mW (i)	165
0.635	Pr	250 mW	476 nm; 800 mW (i)	165
0.715	Pr	50 mW	476 nm; 770 mW (i)	167
0.753	Ho	2 mW	647 nm (uc); 370 mW (i)	73
0.810	Tm	130 mW	1053 nm (uc); 800 mW (a)	123
0.850	Er	60 mW	801 nm (uc); 360 mW (a)	168
0.980	Er	10 mW	647 nm; 300 mW (i)	169
1.02	Yb	85 mW	911 nm; 200 mW (l)	102
1.05	Nd	50 mW	795 nm; 110 mW (l)	103
1.298	Pr	50 mW	1047 nm; 900 mW (i)	104
1.345	Nd	30 mW	795 nm; 110 mW (l)	105
1.47	Tm	1 W	1064 nm (uc); 3.6 W (l)	106
1.72	Er	9 mW	791 nm (uc)	107
1.88	Tm	115 mW	780 nm; 320 mW (l)	108
1.925	Tm	90 mW	790 nm; 300 mW (l)	109
1.963	Tm	8 mW	791 nm; 230 mW (l)	110
2.024	Ho	250 mW	826 nm; 500 mW (l)	111
2.35	Tm	40 mW	790 nm; 300 mW (l)	109
2.79	Er	1.04 W	970 nm; 4.42 W (l)	112
2.9	Ho	12 mW	640 nm; 500 mW (a)	113
3.45	Er	2.5 mW	650 nm; 300 mW (a)	114
3.9	Ho	11 mW (77 K)	885 nm; 900 mW (l)	115

[a] (i) incident, (l) launched, and (a) absorbed pump powers; (uc) up-conversion pumping.

nm with Nd^{3+}-doped ZBLAN fibers.[116,117] The transitions involved are $^4D_{3/2} \rightarrow {}^4I_{11/2}$ and $^2P_{3/2} \rightarrow {}^4I_{11/2}$, as depicted in Figure 5. Excitation of the $^4D_{3/2}$ and $^2P_{3/2}$ levels is obtained by a two-590-nm-photon up-conversion process. Output powers are equal to 74 and 500 μW, with 320 and 275 mW pumping powers, respectively. This UV up-conversion system provides access to applications for which high photon energy and compactness of the laser are of primary importance.

The generation of coherent blue light is a crucial point for application to high-density optical data storage, color displays, laser printing, and medical diagnostics. Blue lasing in fluoride glass fibers was demonstrated at 455 and 481 nm from the $^1D_2$ and $^1G_4$ levels of Tm^{3+} ions. The transitions involved are shown in Figure 8. The highest output of 230 mW is obtained with Tm^{3+} at 481 nm with a 1.6 W pump power at 1123 nm from a mini-YAG:Nd. However, at these high pump powers, the laser performances degrade rapidly because of the presence of color centers. Sanders et al. have demonstrated up-conversion lasing with a Tm^{3+}-doped ZBLAN fiber pumped directly by two high-power laser diodes.[118] With a blue output of 106 mW at 482 nm and a 12% overall conversion efficiency from IR to blue radiation, this system shows promise as a powerful, small-size, all-solid-state blue laser source.

Green coherent light has been obtained as well. Up-conversion of 801 nm light from a single laser diode leads to 3 mW of 544 nm light at the output of an Er^{3+}-doped ZBLAN fiber.[119] Higher output powers are attained with large pump sources such as an Ar^+-pumped dye laser, which permits 38 mW at 549 nm with Ho^{3+}-doped fibers.[120]

Green lasing has been demonstrated in Er^{3+}-doped ZBLAN microspheres.[121] Besides small size, typically $\leq$100 μm, the interest for microspheres is a low laser threshold—30 μW in the present case with up-conversion pumping at 801 nm.

Powerful, compact, all-solid-state red lasers around 635 nm are also demanded for color displays. Compactness of red-emitting systems is achieved by using Yb^{3+}:Pr^{3+} or Nd^{3+}:Pr^{3+} codoped fibers that can be pumped via up-conversion mechanisms. Thus, red lasing at 635 nm with 4.5 mW output power was achieved in an Yb^{3+}:Pr^{3+} ZBLAN fiber pumped by a single laser diode at 860 nm.[122] The incident pump power was 170 mW.

Among the numerous fiber lasers demonstrated in the 700—1050 nm region, one should note the 130 mW thulium laser at 810 nm, a spectral domain where cheap silicon detectors can operate. Pulses as short as 380 ps were generated at that wavelength.[123] In addition, the laser can be tuned from 805 to 820 nm. Lasing with ytterbium-doped fluoride glass fiber is achieved at 1.02 μm with 85 mW output power. The system shows a high slope efficiency of 56% with respect to launched pump power. Neodymium-doped ZBLAN fibers are found to lase at 1.05 μm with quite good efficiency, as expected. A threshold of only 22 mW and a slope efficiency of nearly 60% were reported.[103] Ultrashort pulses from 9 ps to 320 fs were generated in the 1.047—1.060 μm spectral range with an average output of 4 mW from a diode pumped neodymium fluoride glass fiber.[124] Besides optical fibers, continuous-wave (CW) lasing was demonstrated in Nd^{3+}-doped fluoride glass microspheres having diameters ranging from 30 to 500 μm. The system was pumped at 800 nm with a Ti:sapphire laser and lased at 1.05 and 1.33 μm.[125,126]

The only laser oscillation observed in chalcogenide fibers was with Nd^{3+} in GLS glass at 1.08 μm. Output power of 1.2 mW was achieved with 550 mW incident pump power at 1075 nm.[127]

Laser transitions above 1.4 μm belong to the so-called *eye-safe* spectral domain. In this infrared domain, the light is absorbed by the cornea and the lens of the eye, avoiding irreversible damage of the retina. Thulium and erbium ions provide several laser transitions in the 1.4—2.0 μm spectral range. The most significant result, in terms of output power, concerns a Tm^{3+}-doped fluoride fiber that delivers 1 W, continuous-wave, at 1.47 μm. Pumping is at 1.064 μm from a laser-diode-pumped Nd:YAG. The threshold and slope efficiency are 175 mW and 29%, respectively, and wavelength tunability is from 1.445 to 1.51 μm.[106] Komukai et al. demonstrated a high slope efficiency of 59% for 250 mW output and 200 mW threshold.[128] Powerful 1.47-μm lasers are of interest for pumping erbium-doped fiber amplifiers with high gains and high output powers.

Because of the wide transmission range and low phonon energies of fluoride glasses, the observation

of numerous rare-earth laser lines is possible at wavelengths beyond 2 μm, where the transmission of silica fibers is extremely poor. Laser sources around 2 μm are of special interest because they belong not only to the *eye-safe* spectral domain but also to an optical transparency window of the atmosphere. Two fluoride glass fiber lasers have been demonstrated in that region. First, a Ho^{3+} laser with the $^5I_7 \rightarrow {}^5I_8$ transition at 2.024 μm delivers 250 mW with 60% slope efficiency.[111] The ZBLAN fiber is actually codoped with thulium ions to take advantage of efficient energy transfer from the $^3F_4$ (Tm) level to $^5I_7$ (Ho) when pumping at 826 nm from a Ti: sapphire laser. The 2.35 μm transition of Tm^{3+} ions, from $^3H_4$ to $^3H_5$, was also observed in fluoride glass fibers. Like the Ho^{3+} laser at 2.04 μm, this Tm^{3+} fiber laser is within the optical transparency domain of the atmosphere and is susceptible to find applications in lidar technologies. Surgery is another domain of applications for 2 μm lasers because tissue coagulation is favored at this wavelength.

Resonant with the O−H absorption band, the 2.79 μm laser with Er^{3+} ions and the 2.9 μm laser with Ho^{3+} can also be applied in laser surgery as well as in dermatology and dental drilling. High-quality cutting or ablation has been demonstrated in biological tissue, which explains the increasing interest for such lasers operating at ~3 μm.[129,130] The transitions take place between the $^4I_{11/2}$ and $^4I_{13/2}$ levels of erbium and from $^5I_6$ to $^5I_7$ in Ho^{3+}, as depicted in Figure 7. The highest output power is reported for the erbium fluoride glass laser with a record value of 1.04 W, the slope efficiency being 25%.[112] Pumping is at 970 nm with a laser diodes. Even though much more modest in terms of output power (12 mW), the Ho^{3+} fluoride glass laser provides broad tunability from 2.83 to 2.95 μm.

The only glass lasers ever achieved at wavelengths >3 μm are a 3.45 μm Er^{3+}-doped fluoride fiber laser and a 3.9 μm Ho^{3+} laser.[114,115] They correspond to the $^4F_{9/2} \rightarrow {}^4I_{9/2}$ and $^5I_5 \rightarrow {}^5I_6$ transitions shown in Figure 7 and are pumped at 650 and 885 nm, respectively. An output power of 2.5 mW is obtained in CW mode at 3.45 μm. The position of the lasing wavelength is found to be temperature-dependent. Therefore, tuning can be achieved from 3.456 μm at 5 °C up to 3.478 μm at 29 °C. This laser line is in the absorption range of various hydrocarbon groups, the C−H absorption being typically located at ~3.5 μm. This opens possibilities for the monitoring of trace gases and common pollutants.

Contrary to all of the laser lines reported in Table 7, lasing at 3.9 μm with a ZBLAN:Ho^{3+} fiber is achieved at liquid-nitrogen temperature. CW output power of 11 mW is obtained with 900 mW launched pump power at 885 nm. It must be noted that such lasers are of importance for military and space applications because they emit within an atmospheric window that is transparent from 3 to 5 μm. Few lasers exist in this spectral region.

All of the results above were obtained with optical cavities of the Fabry−Perot type with two external dielectric mirrors butted against the fiber ends. More sophisticated systems take advantage of Bragg gratings written directly inside the fluoride glass optical fibers. Permanent Bragg gratings can be photoinduced in cerium-doped fluorozirconate glass plates and fibers by means of conventional holographic interferometry of 246 nm light from a pulsed UV laser.[131] Refractive index changes up to 4×10^{-4} and reflectivity of nearly 100% are achieved. Similar experiments have been conducted with Eu^{2+}- and Ce^{3+}-doped PZG thin films illuminated by a CW laser at 244 nm. Photoinduced modifications of the refractive index were as high as 1.3×10^{-2} and 3.9×10^{-3}, respectively.[132]

2. Optical Amplifiers for Telecommunications

Optical amplifiers are essential components for the development of high-capacity telecommunication networks based on silica optical fibers. Silica fibers are characterized by a low-loss optical window that ranges from 1.2 to 1.7 μm. That window is divided into the ultrashort (XS), short (S), conventional (C), and long (L) bands as shown in Figure 9. The XS- and S-bands are centered at 1.3 and 1.47 μm, whereas the C- and L-bands are equal to 1530−1565 and 1565−1625 nm, respectively. Amplification in the C- and L-bands is commonly achieved with Er^{3+}-doped silica fibers. On the other hand, amplification at 1.47 and 1.3 μm with Tm^{3+} and Pr^{3+} ions requires the use of materials with lower phonon energy than silica. High-gain optical amplification was demonstrated in the XS-, S-, and C-telecommunication windows with rare-earth-doped fluoride glass fibers. *Real-world* amplifiers have been constructed and commercialized. With an estimated lifetime of >25 years in normal conditions, state-of-the-art fluoride fiber are compatible with long-term applications such as telecommunications.[133] Performances of non-oxide glass amplifiers are listed in Table 8, in terms of maximum gain and pumping conditions.[128,134−137, 170]

Up to now, praseodymium-doped ZBLAN glass fiber appears to be the best compromise for 1.3 μm amplification with lanthanide ions. High-gain, low-noise Pr^{3+}-doped fluoride fiber amplifier modules (PDFA) have been developed by several laboratories around the world. The best performances of first-generation PDFAs, in terms of small-signal gain, were achieved by British Telecom Laboratory and

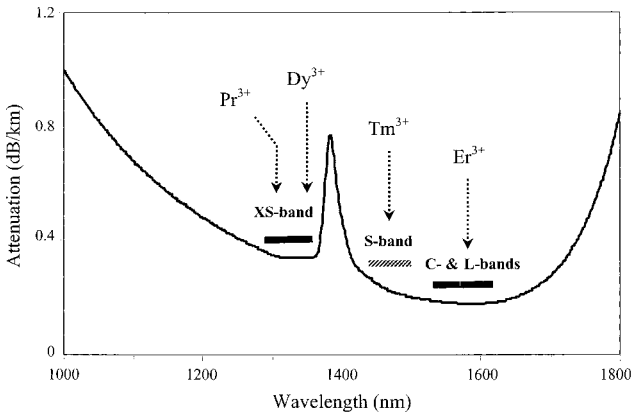

Figure 9. Optical attenuation of silica fibers with position of the telecommunication bands and matching rare-earth emissions.

Table 8. Performances of Optical Amplifiers Based on Lanthanide-Containing Non-Oxide Glass Gibers

λ (μm)	lanthanide	glass	max gain (dB)	pump characteristics	ref
1.3	Pr	ZBLAN	30.5	1.017 μm 500 mW (MOPA)	134
1.3	Pr	fluoroindate (PbF_2-InF_3)	22	1.015 μm 238 mW (MOPA)	135
1.34	Pr	GNS	32	1.017 μm 90 mW (Ti:saph)	136
1.475−1.502	Tm	ZBLAN	>25	1.4 + 1.502 μm (LD)	170
1.54	Er	ZBLAN	33	1.48 μm 50 mW (LD)	137

Nippon Telegraph and Telephone.[138,139] With these amplifiers, a high-power Nd:LYF pump source at 1.047 μm was used. A high gain of 40.6 dB could be attained by means of two amplification units. However, these PDFAs showed low gain coefficients as revealed by the high pump powers required to operate the amplifiers (>650 mW). One reason for such high pump powers is that Nd:LYF emission does not correspond rigorously to the maximum of the $^1G_4$ absorption band. Higher gain coefficients were demonstrated with systems pumped by Ti:sapphire lasers tuned at a more appropriate wavelength of ~1020 nm or specifically designed laser diodes. With these second-generation PDFAs, gains in excess of 20 dB and efficiencies of 0.1−0.2 dB/mW were achieved with launched pump powers of ~300 mW from either InGaAs laser diodes or master oscillator power amplifiers (MOPAs).[140,141] Taking advantage of better pumping conditions, Yamada at al. have constructed a MOPA-pumped PDFA module having a Pr^{3+} fiber that is only 10 m in length. This is to be compared with the 20 m fiber length needed in an equivalent module pumped by Nd:LYF. A gain of 30 dB with 500 mW launched pump power was achieved in this configuration.[134] PDFAs have been successfully implemented in test systems for local communication such as multichannel CATV, for example.[142]

Besides the issue of pump wavelength adequacy, the low quantum efficiency of the 1.3 μm transition of Pr^{3+} ions accounts for the relatively small gain coefficients and high pump powers of PDFAs. This transition is highly phonon-dependent, so its quantum efficiency can be increased by employing glass hosts with phonon energies lower than that of ZBLAN. Thus, lead fluoroindate glasses were developed, and more efficient PDFAs are now available with 20 dB net gain at only 100 mW pump power from a 1015 nm MOPA.[135,143] A gain coefficient as high as 0.36 dB/mW is reported for single-pass amplification. A compact, plug-in type module pumped by laser diodes was developed.[144] The system is capable of delivering a 24 dB small-signal gain. Recently, lead fluoroindate PDFAs have been successfully utilized for data transmission at a 2.5 Gb/s rate over >100 km.[145] A high gain coefficient of 0.81 dB/mW and an efficiency close to 30% were achieved with a praseodymium-doped GNS sulfide glass fiber amplifier.[136] However, refractive index compatibility between sulfide glass and silica remains to be solved for real devices.

Preliminary experiments have recognized Tm^{3+}-doped fluoride glass fiber amplifiers (TDFA) as having a high potential for the S-band, ~1.45 μm. Thus, a primary ZBLAN up-conversion amplifier was demonstrated with a maximum gain of 28 dB at 1.47 μm.[128] Optimization of key parameters such as the fiber length, balance between co- and contra-propagating pumps, has led to improved amplifier characteristics. Thus, a gain of >20dB was demonstrated in the 1453−1483 nm spectral range, with a noise figure of <6 dB.[146] A total pump power of 300 mW was delivered by two laser-diode-pumped Nd:LYF lasers emitting at 1047 nm. A gain-shifted amplifier operating between 1475 and 1502 nm and delivering >25 dB of gain was recently demonstrated.[170] Pumping was achieved by two laser diodes at 1.4 and 1.502 μm. A major drawback of the $^3H_4 \rightarrow {}^3F_4$ transition at 1.47 μm is that the $^3F_4$ lifetime is greater than the $^3H_4$ lifetime (τ_{rad} = 8.7 and 1.7 ms, respectively). In other words, the transition is self-terminating. Therefore, it is necessary to force the depopulation of the terminating level. This can be achieved by an up-conversion pumping mechanism at 1047 nm, the intermediate state of which is $^3F_4$. Another solution consists of codoping with an active ion that shows a coincidental level with $^3F_4$. Theoretical considerations suggest that the upper ^7F_n levels of Tb^{3+} are appropriate for quenching the thulium $^3F_4$ lifetime.

An important result obtained by Alcatel Research is the world record of power conversion efficiency—50%—in a gain-shifted thulium-doped fluoride fiber amplifier pumped at 1238 and 1400 nm.[147] The pump wavelengths were provided by a single Yb^{3+}-fiber laser emitting at 1117 nm coupled to a Raman resonator.

A net optical gain of 33 dB was achieved with Er^{3+}-doped ZBLAN optical amplifiers for the third telecommunication window at 1.54 μm.[137] This gain was obtained with only a 50 mW pump power at 1.48 μm, which resulted in a gain efficiency of 0.86 dB/mW. These fundamental characteristics are not as good as those reported for silica erbium-doped fiber amplifiers (EDFA). However, compared with silica amplifiers, fluoride EDFAs remain of practical interest because they possess a flat and broad gain bandwidth as a function of signal wavelength. This property, which is fundamental for wavelength division multiplexing (WDM), is depicted in Figure 10. This figure shows the optical spectrum of 16 channels at the output of four cascaded fluoride and silica EDFAs without any spectral filtering.[148] One may note that all channels, which range from 1533.7 to 1558.2 nm, are quasi-equally amplified by fluoride EDFAs with a maximum gain variation of 3 dB only. With silica EDFAs, on the other hand, large discrepancies are observed. The gain variation between minimum and maximum amplified channels is as high as 23 dB in that case. Consequently, spectral filtering has to be added to silica EDFAs in practical systems, contrary to fluoride EDFAs. Laboratory tests have demonstrated the transmission of such 16 channels at 10 Gbits/s over 531 km with seven fluoride EDFAs.[149]

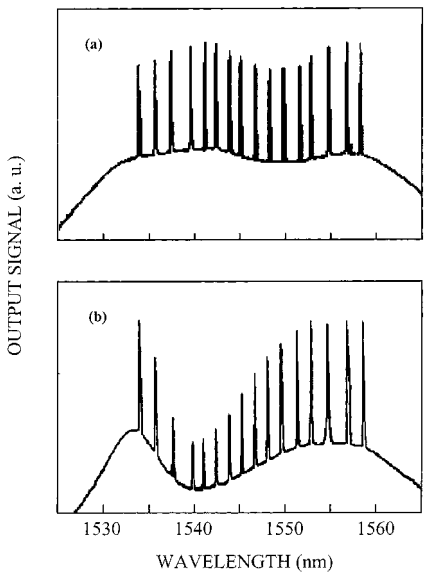

Figure 10. Optical spectrum of 16 channels at the output of four cascaded EDFAs: (a) fluoride amplifier; (b) silica amplifier.

Because of the growing demand for high-speed and high-capacity telecommunication networks, intensive research is devoted to ultra-broadband amplifiers within the entire 1.2−1.7 μm spectral range. Several combinations involving lanthanide-based amplifiers together with Raman amplifiers have been proposed. Thus, in the 1.55 μm domain, an amplifier unit composed of three silica-based EDFAs and one fluoride-based EDFA, in parallel/cascade configuration, shows flat amplification from 1530 to 1560 nm and from 1576 to 1600 nm. Within these bands, an optical gain of 30 dB is achieved with a maximum fluctuation of <1.7 dB.[150] Combination of fluoride-based EDFAs and fiber Raman amplifiers leads to a 67-nm bandwidth amplifying unit that operates from 1534 to 1601 nm.[151] More recently, a record cumulated bandwidth of 17.7 THz over the 1297−1604 nm range was achieved by combining C- and L-bands, silica-based EDFAs, fluoride-based TDFAs for the S-band and Raman amplifiers for the XS-band.[152]

Optical amplification was achieved in Nd^{3+}- and Er^{3+}-doped channel waveguides made of fluoride glasses.[99] Typical results are internal gains of 2.7 dB/cm at 1.047 μm for the neodymium waveguide and 1.6 dB/cm at 1.53 μm for the erbium waveguide.

3. Other Applications of Lanthanides in Fluoride Glasses

Fluoride glasses containing lanthanide(III) ions are suitable for other specific applications that require laser transitions at wavelengths >2 μm, efficient up-conversion mechanisms, or ultrahigh quantum efficiencies.

Some studies were devoted to Tm^{3+}-doped fluoride fibers for hydrocarbon gas sensing, especially CH_4 with regard to safety issues. A thulium fiber laser butt-coupled to a silica fiber Bragg grating was designed to take advantage of the broad tunability of the $^3H_4 \rightarrow {}^3H_5$ transition of Tm^{3+} around 2.3 μm, where methane shows two strong absorption peaks. The sensor, the principle of which is based on the direct absorption of laser light by CH_4, presents a minimum gas detection of 100 ppm·m.[153] Other sensing applications include water sensing by direct absorption of the $^3H_4 \rightarrow {}^3F_4$ transition of Tm^{3+} at 1.47 μm[154] and alcohol sensing by evanescent wave spectroscopy in undoped fluoride glass fibers.[155]

The exceptional efficiency of up-conversion mechanisms in fluoride glasses has been utilized for realizing three-dimensional solid-state color displays. The blue, green, and red colors are obtained with Tm^{3+}, Er^{3+}, and Pr^{3+} ions, respectively. Each color is created by pumping with two infrared laser diodes operating at different wavelengths. The two beams intersect inside the glass volume, producing a luminescent point. Finally, the three dimensional effect is obtained by monitoring the position of the luminescent point by means of fast-scanning mirrors.[156]

Laser-induced cooling is another domain of application for lanthanides in non-oxide glasses. The fundamental principle of laser-induced cooling is anti-Stokes luminescence, that is, luminescence that occurs at a wavelength shorter than that of the pump laser. The energy mismatch is then provided by absorption of phonons in the glass host, which results in a cooling of that host. The cooling efficiency is quite low, so radiative transitions with quantum efficiencies near unity are to be used. From this point of view, the best combinations are obtained with rare-earth ions with large energy gaps between the first excited state and the ground state, embedded in low-phonon-energy hosts. Thus, cooling by 21 K starting from room temperature was demonstrated in a Yb^{3+} (1 wt %) -doped ZBLAN fiber in a vacuum. The fiber was pumped by a Ti:sapphire laser with 1360 mW power at 1015 nm.[157] The phenomenon was also observed in bulk fluoroindate and fluorochloride glasses.[158,159] Modelization has shown that it is possible to cool an internal volume from room temperature to 77 K in Yb-doped fluorochloride glass with a penalty of 20% in the cooling efficiency.[160] Hoyt et al. have observed net cooling in Tm^{3+}-doped fluorozirconate glass for the first time.[161] With pump excitation at 1.9 μm and an incident average power of nearly 3 W, the sample was cooled to −1.2 °C from room temperature.

VI. Conclusion

In summary, lanthanides in non-oxide glasses are unique chemical combinations that have been studied from a fundamental viewpoint as well as for optical applications. Lanthanide(III) ions in fluorozirconate glasses were found to be essentially eight-coordinated and to belong to the glass-forming network. In sulfochloride glass, it was shown that chloride ions surround preferentially the lanthanide ions.

A large number of laser emissions can be obtained with fluoride fibers doped with lanthanides. They may find applications in systems where compact solid state laser sources emitting at wavelengths ranging from the blue to the mid-infrared are needed. The fact that permanent Bragg gratings could be induced in ZBLAN optical fibers is a definite advantage for

the development of compact, all-solid-state fluoride glass fiber lasers involving lanthanides.

From a materials point of view, amplification at 1.3 μm and up-conversion processes benefit from the use of glasses with lower phonon energies than fluorides. Thus, sulfide glasses are for the moment the most exciting materials for the next generation of infrared fiber lasers and amplifiers based on lanthanides.

VII. References

(1) Rault, G.; Adam, J. L.; Smektala, F.; Lucas, J. *J. Fluorine Chem.* **2001**, *110*, 165.
(2) Gao, Y.; Perrot, O.; Boulard, B.; Broquin, J. E.; Rimet, R.; Jacoboni, C. *J. Non-Cryst. Solids* **1997**, *213−214*, 137.
(3) Henriel-Ricordel, C.; Adam, J. L.; Boulard, B.; Sourisseau, C. *Eur. J. Solid State Inorg. Chem.* **1997**, *34*, 125.
(4) Matecki, M.; Poulain, M. *J. Non-Cryst. Solids* **1992**, *140*, 82.
(5) Baniel, P.; Lopez, A.; Gall, P.; Granier, J. *J. Non-Cryst. Solids* **1996**, *203*, 143.
(6) Rigout, N.; Adam, J. L.; Lucas, J. *J. Non-Cryst. Solids* **1993**, *161*, 161.
(7) Messaddeq, Y.; Delben, A.; Aegerter, M. A. *J. Mater. Res.* **1993**, *8*, 885.
(8) Shinn, M. D.; Sibley, W. A.; Drexhage, M. G.; Brown, R. N. *Phys. Rev. B* **1983**, *27*, 6635.
(9) Adam, J.-L.; Ponçon, V.; Lucas, J.; Boulon, G. *J. Non-Cryst. Solids* **1987**, *91*, 191.
(10) Harrison, M. T.; Denning, R. G. *J. Luminesc.* **1996**, *69*, 265.
(11) Soga, K.; Uo, M.; Inoue, H.; Makishima, A.; Inoue, S. *J. Am. Ceram. Soc.* **1995**, *78*, 129.
(12) Balda, R.; Fernandez, J.; Eilers, H.; Yen, W. M. *J. Luminesc.* **1994**, *59*, 81.
(13) Lavin, V.; Rodriguez, D.; Martin, R.; Rodriguez-Mendoza, R. *J. Luminesc.* **1997**, *72−74*, 437.
(14) Nemec, P.; Frumarova, B.; Frumar, M.; Oswald, J. *J. Phys. Chem. Solids* **2000**, *61*, 1583.
(15) Cole, B.; Shaw, L. B.; Pureza, P. C.; Miklos, R.; Sanghera, J. S.; Aggarwal, I. D. *J. Mater. Sci. Lett.* **2000**, *20*, 465.
(16) West, Y. D.; Schweizer, T.; Brady, D. J.; Hewak, D. W. *Fiber Integr. Optics* **2000**, *19*, 229.
(17) Guimond, Y.; Adam, J. L.; Jurdyc, A. M.; Mugnier, J.; Jacquier, B.; Zhang, X. H. *Opt. Mater.* **1999**, *12*, 467.
(18) Rault, G. *Low Phonon-Energy Glasses for Broad Band Optical Amplification*; University of Rennes 1: Rennes, France, 2001.
(19) Clare, A. G. *Key Eng. Mater.* **1994**, *94−95*, 81.
(20) Alves, M. C. M.; Ramos, A. Y.; Watanabe, N. *J. Synchroton Radiat.* **2001**, *8*, 794.
(21) Griscom, L. S.; Adam, J. L.; Binnemans, K. *J. Non-Cryst. Solids* **1998**, *256−257*, 383.
(22) Shin, Y. B.; Heo, J.; Kim, H. S. *J. Mater. Res.* **2001**, *16*, 1318.
(23) Tverjanovich, A.; Tveryanovich, Y. S.; Loheider, S. *J. Non-Cryst. Solids* **1996**, *208*, 49.
(24) Adam, J.-L.; Rigout, N.; Dénoue, E.; Smektala, F.; Lucas, J. *Proc. SPIE−Int. Soc. Opt. Eng.* **1991**, *1581*, 155.
(25) McDougall, J.; Hollis, D. B.; Payne, M. J. P. *Phys. Chem. Glasses* **1994**, *35*, 258.
(26) Binnemans, K.; Görller-Walrand, C.; Adam, J.-L. *Chem. Phys. Lett.* **1997**, *280*, 333.
(27) Görller-Walrand, C.; Binnemans, K. *Handbook on the Physics and Chemistry of Rare Earths*; Elsevier Science: Amsterdam, The Netherlands, 1998; p 101.
(28) Medeiros Neto, J. A.; Hewak, D. W.; Tate, H. *J. Non-Cryst. Solids* **1995**, *183*, 201.
(29) Quimby, R. S.; Miniscalco, W. J. *J. Appl. Phys.* **1994**, *75*, 613.
(30) Goldner, P.; Auzel, F. *J. Appl. Phys.* **1996**, *79*, 7972.
(31) Schweizer, T.; Samson, B. N.; Hector, J. R.; Brocklesby, W. S.; Hewak, D. W.; Payne, D. N. *Infrared Phys. Technol.* **1999**, *40*, 329.
(32) Shin, Y. B.; Jang, J. N.; Heo, J. *Opt. Quantum Electron.* **1995**, *27*, 379.
(33) Shaw, L. B.; Harbison, B. B.; Cole, B.; Sanghera, J. S.; Aggarwal, I. D. *Optics Express* **1997**, *1*, 87.
(34) Schweizer, T.; Hewak, D. W.; et al. *Electron. Lett.* **1996**, *32*, 666.
(35) Hewak, D. W.; Samson, N.; Neto, A. M.; Laming, I.; Payne, D. N. *Electron. Lett.* **1994**, *30*, 968.
(36) Ye, C. C.; Hewak, D. W.; Hempstead, M.; Samson, B. N.; Payne, D. N. *J. Non-Cryst. Solids* **1996**, *208*, 56.
(37) Jurdyc, A. M.; Rault, G.; Meffre, W.; Le Person, J.; Guy, S.; Smektala, F.; Adam, J. L. *Proc. SPIE−Int. Soc. Opt. Eng.* **2002**, *4645*.
(38) Kadono, K.; Yazawa, T.; Shojiya, M.; Kawamoto, Y. *J. Non-Cryst. Solids* **2000**, *274*, 75.
(39) Shin, Y. B.; Cho, Y.; Heo, J. *J. Non-Cryst. Solids* **1996**, *208*, 29.
(40) Cases, R.; Chamarro, M. A. *J. Solid State Chem.* **1991**, *90*, 313.
(41) Seeber, W.; Downing, E. A.; Hesselink, L.; Fejer, M. M.; Ehrt, D. *J. Non-Cryst. Solids* **1995**, *189*, 218.
(42) Adam, J.-L.; Matecki, M.; L'Helgoualch, H.; Jacquier, B. *Eur. J. Solid State Inorg. Chem.* **1994**, *31*, 337.
(43) Nemec, P.; Frumarova, B.; Frumar, M. *J. Non-Cryst. Solids* **2000**, *270*, 137.
(44) Adam, J. L.; Sibley, W. A. *J. Non-Cryst. Solids* **1985**, *76*, 267.
(45) Remillieux, A.; Jacquier, B.; Linarès, C.; Lesergent, C.; Artigaud, S.; Bayard, D.; Hamon, L.; Beylat, J. L. *J. Phys. D: Appl. Phys.* **1996**, *29*, 963.
(46) Arauzo, A. B.; Cases, R.; Alcala, R. *Phys. Chem. Glasses* **1994**, *35*, 202.
(47) Florez, A.; Malta, O. L.; Messaddeq, Y.; Aegerter, M. A. *J. Non-Cryst. Solids* **1997**, *213−214*, 315.
(48) Bunuel, M. A.; Cases, R.; Chamarro, M. A.; Alcala, R. *Phys. Chem. Glasses* **1992**, *33*, 16.
(49) Smart, R. G.; Hanna, D. C.; Tropper, A. C.; Davey, S. T.; Carter, S. F.; Szebesta, D. *Electron. Lett.* **1991**, *27*, 1307.
(50) Hirao, K.; Higuchi, M.; Soga, N. *J. Luminesc.* **1994**, *60−61*, 115.
(51) Quimby, R. S.; Zheng, B. *Appl. Phys. Lett.* **1992**, *60*, 1055.
(52) Xie, P.; Gosnell, T. R. *Electron. Lett.* **1995**, *31*, 191.
(53) Tick, P. A.; Borelli, N. F.; Cornelius, L. K.; Newhouse, M. A. *J. Appl. Phys.* **1995**, *78*, 6367.
(54) Samson, B. N.; Tick, P. A.; Borrelli, N. F. *Opt. Lett.* **2001**, *26*, 145.
(55) Hewak, D. W.; Medeiros Neto, J. A.; Samson, B.; Brown, R. S.; Jedrzejewski, K. P.; J., W.; Taylor, E.; Laming, R. I.; Wylangowski, G.; Payne, D. N. *IEEE Photon. Technol. Lett.* **1994**, *6*, 609.
(56) Balda, R.; Mendioroz, A.; Fernandez, J.; Arriandiaga, M. A.; Griscom, L. S.; Adam, J. L. *Opt. Mater.* **2001**, *16*, 249.
(57) Tesar, A.; Campbell, J.; Weber, M.; Weinzapfel, C.; Lin, Y.; Meissner, H.; Toratani, H. *Opt. Mater.* **1992**, *1*, 217.
(58) Balda, R.; Fernandez, J.; Mendioroz, A.; Adam, J.-L.; Boulard, B. *J. Phys.− Condens. Matter* **1994**, *6*, 913.
(59) Binnemans, K.; Verboven, D.; Görller-Walrand, C.; Lucas, J.; Duhamel-Henry, N.; Adam, J. L. *J. Non-Cryst. Solids* **1996**, *204*, 178.
(60) Schweizer, T. *Properties, Processing and Applications of Glass and Rare-Earth Doped Glasses for Optical Fibres*; INSPEC: London, U.K., 1998; p 320.
(61) Balda, R.; Sanz, M.; Mendioroz, A.; Fernandez, J.; Griscom, L. S.; Adam, J. L. *Phys. Rev. B* **2001**, *64*.
(62) Basiev, T. T.; Dergachev, A. Y.; Orlovskii, Y. V.; Prokhorov, A. M. *J. Luminesc.* **1992**, *53*, 19.
(63) Stanley, A. T.; Harris, E. A.; Searle, T. M.; Parker, J. M. *J. Non-Cryst. Solids* **1993**, *161*, 235.
(64) Adam, J.-L.; Doualan, J.-L.; Griscom, L.; Girard, S.; Moncorgé, R. *J. Non-Cryst. Solids* **1999**, *256−257*, 276.
(65) Adam, J.-L.; Docq, A.-D.; Lucas, J. *J. Solid State Chem.* **1988**, *75*, 403.
(66) Reisfeld, R.; Eyal, M.; Jacoboni, C.; Jørgensen, C. K. *Chimia* **1988**, *42*, 145.
(67) Tanabe, S.; Hanada, T.; Watanabe, M.; Hayashi, T.; Soga, N. *J. Am. Ceram. Soc.* **1995**, *78*, 2917.
(68) Cases, R.; Chamarro, M. A.; Alcalá, R.; Rodriguez, V. D. *J. Luminesc.* **1991**, *48−49*, 509.
(69) Schweitzer, T.; Hewak, D. W.; Samson, B. N.; Payne, D. N. *Opt. Lett.* **1996**, *21*, 1594.
(70) Tanimura, K.; Shinn, M. D.; Sibley, W. A.; Drexhage, M. G.; Brown, R. N. *Phys. Rev. B* **1984**, *30*, 2429.
(71) Villacampa, B.; Orera, V. M.; Merino, R. I.; Cases, R.; Alonso, P. J.; Alcalá, R. *Mater. Res. Bull.* **1991**, *26*, 741.
(72) Binnemans, K.; Görller-Walrand, C.; Lucas, J.; Duhamel, N.; Adam, J. L. *J. Alloys Compd.* **1995**, *225*, 80.
(73) Allain, J. Y.; Monerie, M.; Poignant, H. *Electron. Lett.* **1990**, *26*, 261.
(74) Zou, X.; Toratani, H. *J. Non-Cryst. Solids* **1996**, *201*, 37.
(75) Zou, X.; Toratani, H. *J. Non-Cryst. Solids* **1995**, *181*, 87.
(76) Adam, J.-L.; Guéry, C.; Lucas, J.; Rubin, J.; Moine, B.; Boulon, G. *Mater. Sci. Forum* **1987**, *19−20*, 573.
(77) Tanabe, S.; Takahara, K.; Takahashi, M.; Kawamoto, Y. *J. Opt. Soc. Am. B* **1995**, *12*, 786.
(78) McDougall, J.; Hollis, B.; Payne, J. *Phys. Chem. Glasses* **1996**, *37*, 256.
(79) Takahashi, M.; Shojiya, M.; Kanno, R.; Kawamoto, Y.; Kadono, K.; Ohtsuki, T.; Peyghambarian, N. *J. Appl. Phys.* **1997**, *81*, 2940.
(80) Bell, M. J. V.; deSousa, D. F.; Nunes, L. A. O. *J. Appl. Phys.* **2000**, *87*, 8264.
(81) Cho, W. J.; Kim, M. W.; Jo, J. C.; Choi, S. S.; Park, S. J. *Jpn. J. Appl. Phys.* **1994**, *33*, L1527.
(82) Catunda, T.; Nunez, L. A. O.; Florez, A.; Messaddeq, Y.; Aegerter, M. A. *Phys. Rev. B* **1996**, *53*, 6065.
(83) de Araujo, C. B.; Menezes, L. S.; Maciel, G. S.; Acioli, L. H.; Gomes, A. S. L.; Messaddeq, Y.; Florez, A.; Aegerter, M. A. *Appl. Phys. Lett.* **1996**, *68*, 602.

(84) Pope, C. L.; Reddy, B. R.; Nash-Stevenson, S. K. *Opt. Lett.* **1997**, *22*, 295.
(85) Yeh, D. C.; Sibley, W. A.; Schneider, I.; Afzal, R. S.; Aggarwal, I. *J. Appl. Phys.* **1991**, *69*, 1648.
(86) Sandrock, T.; Diening, A.; Huber, G. *Opt. Lett.* **1999**, *24*, 382.
(87) Guimond, Y.; Adam, J. L.; Jurdyc, A. M.; Ma, H. L.; Mugnier, J.; Jacquier, B. *J. Non-Cryst. Solids* **1999**, *257*, 378.
(88) Kadono, K.; Higuchi, H.; Takahashi, M.; Kawamoto, Y.; Tanaka, H. *J. Non-Cryst. Solids* **1995**, *184*, 309.
(89) Sanz, J.; Cases, R.; Alcalá, R. *J. Non-Cryst. Solids* **1987**, *93*, 377.
(90) Guéry, C.; Adam, J.-L.; Lucas, J. *J. Luminesc.* **1988**, *42*, 181.
(91) Miazato, K.; deSousa, D. F.; Delben, A.; Delben, J. R.; deOliveira, S. L.; Nunes, L. A. O. *J. Non-Cryst. Solids* **2000**, *273*, 246.
(92) Tanabe, S.; Hanada, T. *J. Appl. Phys.* **1994**, *76*, 3730.
(93) Jacquier, B.; Linarès, C.; Mahiou, R.; Adam, J.-L.; Dénoue, E.; Lucas, J. *J. Luminesc.* **1994**, *60*−*61*, 175.
(94) Kermaoui, A.; Denis, J. P.; Özen, G.; Goldner, P.; Pellé, F.; Blanzat, B. *Opt. Commun.* **1994**, *110*, 581.
(95) Adam, J. L. *Encyclopedia of Materials: Science and Technology*; Elsevier Science: Amsterdam, The Netherlands, 2001; p 3559.
(96) Cole, B.; Shaw, L. B.; Pureza, P. C.; Mossadegh, R.; Sanghera, J. S.; Aggarwal, I. D. *J. Non-Cryst. Solids* **1999**, *257*, 253.
(97) Adam, J. L.; Lucas, J. *Proc. SPIE*−*Int. Soc. Opt. Eng.* **1999**, *3622*, 32.
(98) Szebesta, D.; Davey, S. T.; Williams, J. R.; Moore, M. W. *J. Non-Cryst. Solids* **1993**, *161*, 18.
(99) Adam, J. L.; Lebrasseur, E.; Boulard, B.; Jacquier, B.; Fonteneau, G.; Gao, Y.; Sramek, R.; Legein, C.; Guy, S. *Proc. SPIE*−*Int. Soc. Opt. Eng.* **2000**, *3942*, 130.
(100) Boulard, B.; Coste, S.; Gao, Y.; Legein, C.; Dugopolovski, C. *J. Non-Cryst. Solids* **2000**, *276*, 72.
(101) Adam, J.-L. *Advanced Inorganic Fluorides: Synthesis, Characterization and Applications*; Elsevier: Amsterdam, The Netherlands, 2000; p 235.
(102) Allain, J. Y.; Monerie, M.; Poignant, H. *Electron. Lett.* **1992**, *28*, 988.
(103) Brierley, M. C.; Hunt, M. H. *Proc. SPIE*−*Int. Soc. Opt. Eng.* **1989**, *1171*, 157.
(104) Döring, H.; Peupelmann, J.; Wenzel, F. *Electron. Lett.* **1995**, *31*, 1068.
(105) Millar, C. A.; Fleming, S. C.; Brierley, M. C.; Hunt, M. H. *IEEE Photon. Technol. Lett.* **1990**, *2*, 415.
(106) Miyajima, Y.; Komukai, T.; Sugawa, T. *Electron. Lett.* **1993**, *29*, 660.
(107) Pollnau, M.; Ghisler, C.; Bunea, G.; Bunea, M.; Lüthy, W.; Weber, H. P. *Appl. Phys. Lett.* **1995**, *66*, 3564.
(108) Percival, R. M.; Szebesta, D.; Davey, S. T. *Electron. Lett.* **1992**, *28*, 1866.
(109) Percival, R. M.; Szebesta, D.; Davey, S. T. *Electron. Lett.* **1992**, *28*, 671.
(110) Smart, R. G.; Carter, J. N.; Tropper, A. C.; Hanna, D. C. *Opt. Commun.* **1991**, *82*, 563.
(111) Percival, R. M.; Szebesta, D.; Davey, S. T.; Swain, N. A.; King, T. A. *Electron. Lett.* **1992**, *28*, 2231.
(112) Sandrock, T.; Fischer, D.; Glas, P.; Leitner, M.; Wrage, M.; Diening, A. *Opt. Lett.* **1999**, *24*, 1284.
(113) Wetenkamp, L. *Electron. Lett.* **1990**, *26*, 883.
(114) Többen, H. *Electron. Lett.* **1993**, *29*, 667.
(115) Schneider, J.; Carbonnier, C.; Unrau, U. B. *Appl. Opt.* **1997**, *36*, 8595.
(116) Funk, D. S.; Carlson, J. W.; Eden, J. G. *Electron. Lett.* **1994**, *30*, 1859.
(117) Funk, D. S.; Carlson, J. W.; Eden, J. G. *Opt. Lett.* **1995**, *20*, 1474.
(118) Sanders, S.; Waarts, R. G.; Mehuys, D. G.; Welch, D. F. *Appl. Phys. Lett.* **1995**, *67*, 1815.
(119) Massicott, J. F.; Brierley, M. C.; Wyatt, R.; Davey, S. T.; Szebesta, D. *Electron. Lett.* **1993**, *29*, 2119.
(120) Funk, D. S.; Stevens, S. B.; Wu, S. S.; Eden, J. G. *IEEE J. Quantum Electron.* **1996**, *32*, 638.
(121) von Klitzing, W.; Jahier, E.; Long, R.; Lissillour, F.; Lefèvre-Seguin, V.; Hare, J.; Raimond, J. M.; Haroche, S. *J. Opt. B: Quantum Semiclassical Opt.* **2000**, *2*, 204.
(122) Baney, D. M.; Yang, L.; Ratcliff, J.; Chang, K. W. *Electron. Lett.* **1995**, *31*, 1842.
(123) Yang, L. M.; Walton, D. T.; Nees, J.; Weber, W. H. *Electron. Lett.* **1996**, *32*, 658.
(124) Wegmüller, M.; Schürch, M.; Hodel, W.; Weber, H. P. *IEEE J. Quantum Electron.* **1998**, *34*, 14.
(125) Miura, K.; Tanaka, K.; Hirao, K. *J. Non-Cryst. Solids* **1997**, *213*−*214*, 276.
(126) Fujiwara, H.; Sasaki, K. *J. Appl. Phys.* **1999**, *86*, 2385.
(127) Schweizer, T.; Samson, B. N.; Moore, R. C.; Hewak, D. W.; Payne, D. N. *Electron. Lett.* **1997**, *33*, 414.
(128) Komukai, T.; Yamamoto, T.; Sugawa, T.; Miyajima, Y. *IEEE J. Quantum Electron.* **1995**, *31*, 1880.
(129) Pollnau, M.; Jackson, S. D. *IEEE J. Sel. Top. Quantum Electron.* **2001**, *7*, 30.
(130) Dickinson, B. C.; Golding, P. S.; Pollnau, M.; King, T. A.; Jackson, S. D. *Opt. Commun.* **2001**, *191*, 315.
(131) Poignant, H.; Boj, S.; Delevaque, E.; Monerie, M.; Taunay, T.; Niay, P.; Bernage, P.; Xie, W. X. *Electron. Lett.* **1994**, *30*, 1339.
(132) Xie, W. X.; Bernage, P.; Ramecourt, D.; Douay, M.; Taunay, T.; Niay, P.; Boulard, B.; Gao, Y.; Jacoboni, C.; Da Costa, A.; Poignant, H.; Monerie, M. *Opt. Commun.* **1997**, *134*, 36.
(133) Fujiura, K.; Nishida, Y.; Kanamori, T.; Terunuma, Y.; Hoshino, K.; Nakagawa, K.; Ohishi, Y.; Sudo, S. *IEEE Photon. Technol. Lett.* **1998**, *10*, 946.
(134) Yamada, M.; Kanamori, T.; Ohishi, Y.; Shimizu, M.; Terunuma, Y.; Sato, S.; Sudo, S. *IEEE Photon. Technol. Lett.* **1997**, *9*, 321.
(135) Nishida, Y.; Kanamori, T.; Ohishi, Y.; Yamada, M.; Kobayashi, K.; Sudo, S. *IEEE Photon. Technol. Lett.* **1997**, *9*, 318.
(136) Tawarayama, H. *Properties, Processing and Applications of Glass and Rare-Earth Doped Glasses for Optical Fibres*; INSPEC: London, U.K., 1998; p 355.
(137) Miyajima, Y.; Komukai, T.; Sugawa, T.; Yamamoto, T. *Opt. Fiber Technol.* **1994**, *1*, 35.
(138) Whitley, T. J. *J. Lightwave Technol.* **1995**, *13*, 744.
(139) Yamada, M.; Shimizu, M.; Kanamori, T.; Ohishi, Y.; Terunuma, Y.; Oikawa, K.; Yoshinaga, H.; Kikushima, K.; Miyamoto, Y.; Sudo, S. *IEEE Photon. Technol. Lett.* **1995**, *7*, 869.
(140) Shimizu, M.; Kanamori, T.; Temmyo, J.; Wada, M.; Yamada, M.; Terunuma, Y.; Ohishi, Y.; Sudo, S. *IEEE Photon. Technol. Lett.* **1993**, *5*, 654.
(141) Sanders, S.; Dzurko, K.; Parke, R.; O'Brien, S.; Welch, D. F.; Grubb, S. G.; Nykolak, G.; Becker, P. C. *Electron. Lett.* **1996**, *32*, 343.
(142) Yoshinaga, H.; Yamada, M.; Shimizu, M.; Kanamori, T. *Electron. Lett.* **1994**, *30*, 2042.
(143) Nishida, Y.; Yamada, M.; Kanamori, T.; Kobayashi, K.; Temmyo, J.; Sudo, S.; Ohishi, Y. *IEEE J. Quantum Electron.* **1998**, *34*, 1332.
(144) Nishida, Y.; Yamada, M.; Temmyo, J.; Kanamori, T.; Ohishi, Y. *IEEE Photon. Technol. Lett.* **1997**, *9*, 1096.
(145) Isshiki, K.; Kubota, M.; Kuze, Y.; Yamaguchi, S.; Watanabe, H.; Kasahara, K. *IEEE Photon. Technol. Lett.* **1998**, *10*, 1112.
(146) Aozasa, S.; Sakamoto, T.; Kanamori, T.; Hoshino, K.; Kobayashi, K.; Shimizu, M. *IEEE Photon. Technol. Lett.* **2000**, *12*, 1331.
(147) Roy, F.; Leplingard, F.; Lorcy, L.; Le Sauze, A.; Baniel, P.; Bayart, D. *Electron. Lett.* **2001**, *37*, 943.
(148) Clesca, B.; Bayart, D.; Hamon, L.; Beylat, J. L.; Coeurjolly, C.; Berthelon, L. *Electron. Lett.* **1994**, *30*, 586.
(149) Artigaud, S.; Chbat, M.; Nouchi, P.; Chiquet, F.; Bayart, D.; Hamon, L.; Pitel, A.; Goudeseune, F.; Bousselet, P.; Beylat, J.-L. *Electron. Lett.* **1996**, *32*, 1389.
(150) Yamada, M.; Ono, H.; Kanamori, T.; Sudo, S.; Ohishi, Y. *Electron. Lett.* **1997**, *33*, 710.
(151) Kawai, S.; Masuda, H.; Suzuki, K.; Aida, K. *IEEE Photon. Technol. Lett.* **1999**, *11*, 886.
(152) Bayart, D.; Baniel, P.; Bergonzo, A.; Boniort, J. Y.; Bousselet, P.; Gasca, L.; Hamoir, D.; Leplingard, F.; Le Sauze, A.; Nouchi, P.; Roy, F.; Sillard, P. *Electron. Lett.* **2000**, *36*, 1569.
(153) McAleavey, F. J.; J, O. G.; Donegan, J. F.; Hegarty, J.; Maze, G. *Sensors Actuat.* **2001**, *87*, 107.
(154) McAleavey, F. J.; MacCraith, B. D. *Electron. Lett.* **1995**, *31*, 1379.
(155) MacCraith, B. D.; Ruddy, V.; McCabe, S. *Proc. SPIE*−*Int. Soc. Oct. Eng.* **1991**, *1587*, 310.
(156) Downing, E. A.; Hesselink, L.; Ralston, J.; Macfarlane, R. M. *Science* **1996**, *273*, 1185.
(157) Luo, X.; Eisaman, M. D.; Gosnell, T. R. *Opt. Lett.* **1998**, *23*, 639.
(158) Murtagh, M. T.; Sigel, G. H.; Fajardo, J. C.; Edwards, B. C.; Epstein, R. I. *J. Non-Cryst. Solids* **1999**, *253*, 50.
(159) Fernandez, J.; Mendioroz, A.; Garcia, A. J.; Balda, R.; Adam, J. L. *Phys. Rev. B* **2000**, *62*, 3213.
(160) Fernandez, J.; Balda, R.; Mendioroz, A.; Sanz, M.; Adam, J. L. *J. Non-Cryst. Solids* **2001**, *287*, 437.
(161) Hoyt, C. W.; Sheik-Bahae, M.; Epstein, R. I.; Edwards, B. C.; Anderson, J. E. *Phys. Rev. Lett.* **2000**, *85*, 3600.
(162) Le Flohic, M. P.; Allain, J. Y.; Stéphan, G. M.; Mazé, G. *Opt. Lett.* **1994**, *19*, 1982.
(163) Paschotta, R.; Moore, N.; Clarkson, W. A.; Tropper, A. C.; Hanna, D. C.; Maze, G. *IEEE J. Sel. Top. Quantum Electron.* **1997**, *3*, 1100.
(164) Zhao, Y.; Fleming, S.; Poole, S. *Opt. Commun.* **1995**, *114*, 285.
(165) Smart, R. G.; Carter, J. N.; Tropper, A. C.; Hanna, D. C.; Davey, S. T.; Carter, S. F.; Szebesta, D. *Opt. Commun.* **1991**, *86*, 333.
(166) Whitley, T. J.; Millar, C. A.; Wyatt, R.; Brierley, M. C.; Szebesta, D. *Electron. Lett.* **1991**, *27*, 1785.
(167) Allain, J. Y.; Monerie, M.; Poignant, H. *Electron. Lett.* **1991**, *27*, 189.
(168) Millar, C. A.; Brierley, M. C.; Hunt, M. H.; Carter, S. F. *Electron. Lett.* **1990**, *26*, 1871.
(169) Allain, J. Y.; Monerie, M.; Poignant, H. *Electron. Lett.* **1989**, *25*, 1082.
(170) Kasamatsu, T.; Yano, Y.; Ono, T. *Electron. Lett.* **2000**, *36*, 1607.

CR010305B